JJMIE

Volume 17, Number 4, December. 2023
ISSN 1995-6665
Pages 625– 643
https://doi.org/10.59038/jjmie/170417
Editor-in-Chief: Prof. Ali M. Jawarneh

Jordan Journal of Mechanical and Industrial Engineering

Parametric Study and Optimization of Inconel 625 Processing by ANN and Desirability Function Approach During Graphite Mixed EDM

Sovan Bhowmick[a], Binod Barai[a], Debismita Naik[b], Subhasish Sarkar[a,*], Nisantika Biswas[c], Swapan Kumar Maity[d], Gautam Majumdar[a]

[a] *Mechanical Engineering Department, Jadavpur University, Kolkata, West Bengal 700032, India.*
[b] *Department of Physical Sciences, Indian Institute of Science Education and Research, Kolkata, West Bengal 741246, India.*
[c] *Department of Mechanical Engineering, Academy of Technology, Hooghly, West Bengal 712502, India.*
[d] *Professor, Maulana Abul Kalam Azad University of Technology, West Bengal, Haringhata, West Bengal 741249*

Received 12 Jun 2023 *Accepted 15 Sep 2023*

Abstract

In the present research, electric discharge machining (EDM) was performed on Inconel 625, a nickel-based superalloy by mixing graphite micro powder in dielectric fluid during machining. A Box-Behnken type RSM design was constructed for the experimental work varying five input parameters viz. current, pulse on time, duty cycle, powder concentration and mesh size of the powder to study their effects on material removal rate (MRR), tool wear rate (TWR) and surface roughness (SR). Further, back propagation type artificial neural network (ANN) was developed, trained and tested with the experimental data. Multi response desirability function was applied to the RSM model to maximize MRR, optimize TWR at a stipulated target value and minimize SR. The analysis of the experimental result indicates that current and powder concentration have the extreme influence on all the three responses.The obtained ANN model provides a mean error of prediction as 5.95%, 7.30% and 6.40% for MRR, TWR and SR respectively. The overall R value of the model is found as 0.945 which indicates that the ANN model is adequate to predict the responses for other combination of input parameters. From the desirability function analysis, the optimized value of MRR, TWR and SR are found as 26.135 mm^3/min, 0.0800 mm^3/min and 5.81 µm at current = 8.6 A, pulse on time = 35 µs, duty cycle = 0.5, powder concentration = 8 g/l and mesh size at 35 µm. The study of surface characterization of the Inconel 625 samples have been performed using AFM, SEM and XRD analysis. The AFM and SEM study revealed that the surface irregularities and the width of microcracks increase continuously with the increase of current.

Keywords: EDM, MRR, surface roughness, TWR, ANN, SEM, XRD.

1. Introduction

In recent days, the demand for non-ferrous superalloys is increasing rapidly because of their light weight compared to ferrous alloy and magnificent mechanical properties. Inconel is a nickel-based ferrous alloy which is used in different engineering sectors such as aerospace, gas turbine manufacturing, nuclear power plant and automotive [1]. The high tensile strength, hardness, fatigue life and nearly zero corrosion rate made this alloy so demanding in these manufacturing industries. Inconel is also used in high-temperature applications since it retains almost all the mechanical properties at the elevated temperature [2]. With the increase of demand, the processing of materials needs to be more efficient for enhancing productivity [3]. Since the conventional way of Inconel processing is pretty poor, many non-conventional machining processes are used to cut the material. Electric discharge machining (EDM) is one of the convenient way that is highly used for Inconel processing [4].

EDM is a non-conventional machining process where material is removed by applying a series of high-energy electrical sparks at the gap of the electrode and the work surface. The high-energy spark generates temperature beyond the melting point of the material. The high temperature melts and removes the materials by forming a small crater on the surface [5]. In this process, no mechanical contact is established between the tool and the workpiece which makes it advantageous to machine any difficult to cut materials [6, 7]. However, the rate of material removal is very low and the surface unevenness is very high compared to conventional machining processes [8]. Several researches are performed to overcome the challenges like addition of different technologies, parametric optimization and many more. Powder mixed electric discharge machining (PMEDM) is a new technology which is proven efficient to improve the machining quality and material removal rate. In this process, tiny little electrically conductive particles are mixed with dielectric fluid used in EDM and applied before the machining. During the process, the particles arrange themselves in the form of chains at the spark gap. When the voltage is applied between the

* Corresponding author e-mail: subha.jumechanical@yahoo.com.

electrode and workpiece, the particles get electrically induced and start discharging with move in a random path. This enhances the thermal conductivity of the dielectric medium and widen the spark gap when the main spark is applied [9]. Several local sparks along with the main spark increase the material removal rate, surface roughness and tool wear rate during the machining. Several researches have been conducted on powder mixed electric discharge machining and found that the MRR, surface roughness and surface morphological characteristics are enhanced with different combination of process parameters. Majumdar et al. [10] studied the effect of graphene nano powder on Inconel 625 during the PMEDM. Three process parameters such as current, powder concentration and pulse on time have been selected as process parameters and studied their effects on MRR. The result indicates that the maximum MRR was found at a graphene concentration of 0.4 weight %. Talla et al. [11] analyzed the PMEDM study on Inconel 625 with three different powders viz. graphite, silicon and aluminium. MRR, surface roughness, microhardness and overcut have been studied in this research. In the result, the best MRR was found during the graphite mixed EDM whereas the best surface quality, microhardness and least overcut have been found during silicon mixed EDM.A research was conducted where silicon powder of mesh size 10 µm is mixed with EDM oil at 2g/l concentration and applied on AISI H13 steel [12]. In the study, it is found that the surface heterogeneity was significantly reduced and thickness of the white layer became thinner compared to the normal EDM. Kolli and Kumar [13] performed an investigation where graphite powder and span 20 surfactant were added with EDM oil and applied on Ti-6Al-4V alloy for EDM. The result shows that the discharge current and powder concentration mostly affect the MRR and tool wear rate whereas the surface roughness and the recast layer thickness (RLT) are affected by current and surfactant concentration. Another two studies associated with powder mixed EDM [14, 15] were performed by aiming the changes of surface characteristics, surface integrity and formation of micro-cracks after machining. Titanium nano powder mixed dielectric fluid with the concentration of 2 g/l was applied during the machining of AISI D2 steel and found that the MRR and surface roughness were increased and decreased by 69% and 35% respectively for the discharge current of 6A to 12A respectively. In the second research, carbon nanofiber was added to hydrocarbon based dielectric oil at 0 to 0.28 g/l concentration and applied on RB- SiC material for micro EDM. It is observed that the addition of carbon nano fiber helps to reduce the tool concavity, micro-cracks and crater diameter of the surfaces. Talla et al. [16] did multi response optimization using Grey-Relation Analysis during the cutting of Aluminium/Alumina metal matrix composites (MMC) using Al powder (45 µm) mixed kerosene oil. The concentrations of the powder were chosen from 0 to 10 g/l. The study revealed that the high MRR and low surface roughness can be achieved when the parameters were chosen as powder concentration at 6 g/l, current at 3A, pulse on time at 150 µs and duty cycle at 85%. Anitha et al. [17] have used artificial neural network to predict and optimize the EDM process parameters during the machining of AISI D2 steel. In this study, the maximum MRR and minimum SR have been found as 51.58 mm^3/min and 0.14 µm respectively.

Moreover, a research was conducted where magnetic field is applied during PMEDM of aluminium 6061 alloy [18]. In addition to PMEDM, a magnetic field of intensity 0 to 0.458T was applied with aluminium mixed dielectric during cutting. As a result, it was found that the MRR was increased and TWR was decreased with the increase of magnetic field and powder concentration. Sahu and Datta [19] investigated the effects of graphite on the surface morphology of Inconel 718 and compared with normal EDM. The study revealed that the maximum MRR and SR were achieved at 30A and 20A respectively. Also the white layer thickness increases slightly during PMEDM compare to normal EDM. The effects of graphite powder were found efficient for micro EDM in two researches [20,21]. It was observed that the addition of graphite in kerosene increased the MRR and reduced the surface roughness by 30.9% and 28.3% respectively whereas addition with EDM oil in wire cut EDM increased the MRR and spark gap by maximum 33% to 159% respectively. Wong et al. [22] did a different research by developing near mirror finish surface with addition of graphite and silicon powder. The current was kept at 2A and found that the addition of powder improved the surface quality by placing small, shallow and uniform crates on the machined surface. In a similar approach, Xie et al. [23] had performed a special EDM process where TiC coating were imposed on steel using graphite mixed dielectric. The tribological properties like friction and wear were measured and observed that beside the friction and wear, the coating thickness and microhardness increased by addition of graphite powder compared to normal coating.

Recently, different mathematical and predictive models using the concept of machine learning become popular and they are used in the field of manufacturing for mathematical analysis. The RSM desirability functions have been used in a study to minimize the corrosion rate of Aluminium based composite with the optical setting of input parameters [24]. The result shows that the accuracy of the RSM desirability function is more than 90% to optimize the corrosion rate. Rahimi and Fazlollahtabar [25] applied genetic algorithm and particle swarm optimization to optimize the closed loop green supply chain network and compared the two optimization techniques. It was found that genetic algorithm is more efficient than particle swarm optimization technique with respect to relative percentage deviation and solution time. In EDM also, several models have been employed and found efficient for prediction of data. Artificial Neural Network (ANN) was applied in a study of SKD 11 tool steel machining using EDM [26]. In this study, Elman neural network was used to predict the surface roughness and found the mean square error and R value as 0.31355 and 0.999 respectively. Apart from EDM, Hayajneh and Abdellahia [27] applied gene expression programming (GEP) to predict the performance of an end milling parameters. Out of several GEP model applied for the study, the maximum R^2 and minimum mean square error came as 0.928 and 0.268 respectively which determines the model can be accepted. Ayun et al. [28] applied particle swarm algorithm (PSO)to optimize the injection moulding process parameters and the result shows that the parameter shrinkage and warpage has been improved by 2.4233%. In another research, fuzzy predictive models were also employed to predict the responses in EDM process. Adaptive neuro-fuzzy inference system (ANFIS) and Mamdani based fuzzy logic were developed in two experimental results [29, 30] during the EDM of Inconel 718. The ANFIS based fuzzy logic predicted the MRR, surface roughness and TWR with the accuracy of 95.55%, 97.82% and 90.35% respectively. Whereas, the mamdani based fuzzy logic with linear membership function predicted the MRR and surface roughnesswith the accuracy of 89.21% and 91.23% respectively.

The study of literatures shows that there is no significant research work which analyzed the effect of mesh size of graphite powder on the responses. In this study, graphite micro powder was added to EDM oil dielectric fluid at three different concentrations of 2 g/l, 5 g/l and 8 g/l and applied during the machining of Inconel 625. Along with powder concentration, otherinput parameters such as current, pulse on time, duty cycle and powder mesh size were selected in three different levels. Box-Behnken type RSM was used to prepare the experimental table which consists 46 number of experimental

run. The effects of the process parameters were investigated on material removal rate (MRR), tool wear rate (TWR) and surface roughness (SR). Further, a three layer artificial neural network (ANN) was developed using the experimental result. Multi response desirability function was used to obtain the optimize MRR, TWR and SR. Finally, the generated machine surface was analyzed by FESEM and XRD to investigate the surface morphology and phase transformation.

2. Experimentation

2.1. Selection of workpiece, electrode and powder material

Inconel 625 has been selected for workpiece material in this study. It is a nickel based supperalloy that contains around 60% nickel 20% chromium. The chemical composition of the alloy was analyzed by Positive Material Identification testing machine (Makers: Thermo Fisher, Model: XL 2 800, Sr. No: 76526) and listed in Table 1. It has very high tensile strength, hardness and thermal conductivity compared to ferrous alloy. The mechanical, electrical and thermal properties of the material are shown in Table 2. The square plate of Inconel 625 having thickness 1.27 mm has been cut into small pieces of size 15 mm × 15 mm using wire EDM. Before machining, the samples were cleaned with acid solution followed by water. Further they were polished by emery paper (grade 1000) for 10 minutes to remove the dust particles and oil film. In this experiment, copper round bar with 99.5% purity was selected for the electrode material. The diameter and length of the round bar were 12 mm and 100 mm respectively.

Graphite micro powder was added with Carol EDM oil dielectric fluid before conducting the experiment and stirred thoroughly before initiating the discharge. Three size of powder particles were used here viz. 15 µm, 25 µm and 35 µm. The properties of graphite micro powders are listed in Table 3. The mass of the graphite micro powders of each mesh size was measured and then it is mixed in EDM oil.

Table 1. Alloying element percentage of Inconel 625.

Element	Ni	Fe	Cr	Ti	Mo	Nb
%	62.1	4.79	21.30	0.1	8.11	3.68

Table 2. Properties of Inconel 625.

Properties	Density	Tensile Strength	Hardness	Melting Point	Thermal Conductivity	Electrical resistivity	Specific heat
Units	kg/m^3	MPa	(Brinell)	^{0}C	W/mK	µΩ/m	J/g ^{0}C
Values	8440	992.9	210	1320	9.86	1.26	0.402

Table 3. Properties of graphite powder.

Properties	Density	Melting Point	Thermal Conductivity	Electrical conductivity	Specific heat
Units	kg/m^3	^{0}C	W/mK	µΩ^{-1}/cm	J/g ^{0}C
Values	1300	4550	0.25	500	0.714

2.2. Experimental set up

The experiments were conducted in die sinking type electric discharge machine (Model: ENC 20 of 400 × 250 manufactured by Reliable Enterprises, Maharastra, India) with a special arrangement installed inside its dielectric chamber. The special arrangement consists a tank made by acrylic plate having a capacity of 50 liters. Two metallic plates are attached by nut and bolt at the bottom surface to establish the electrical connect between workpiece and the tank. Additionally, one submerged pump and a stirring mechanism are attached in the tank. The submerged pump is required for continuous flushing of the material at the machining area. The stirring mechanism having a motor attached fan blade is used to stir the dielectric fluid continuously. To ensure homogeneity, the stirrer continuously rotates during the machining. During the experiment, 12.12 L EDM oil was stored inside the tank. Then graphite powder of proper mesh size and required amount was mixed with EDM oil and stir it for one hour before machining. The photographic view of the setup is shown in Fig. 1(a) and the schematic representation is shown in Fig. 1(b).

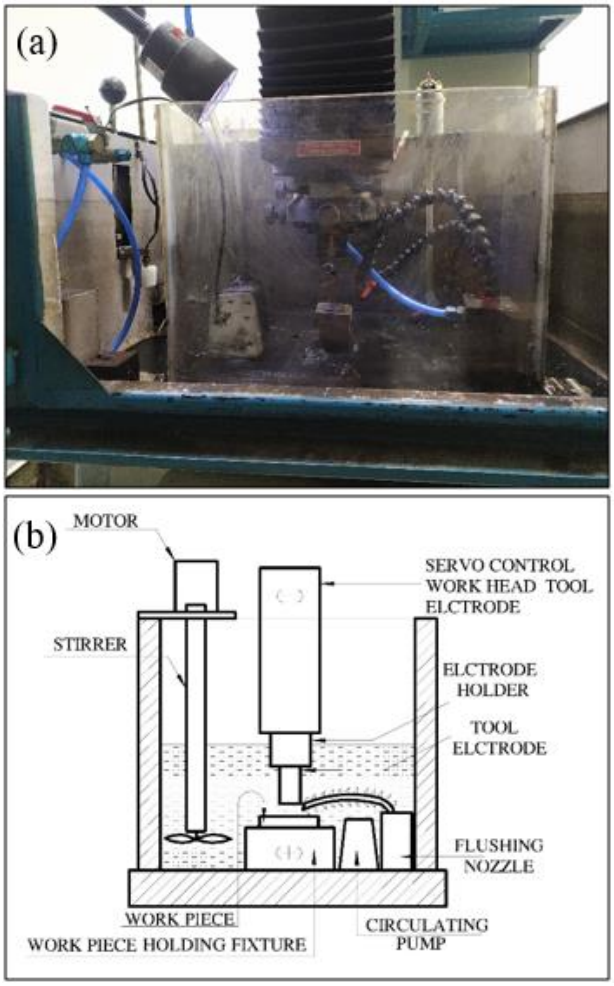

Figure 1. Experimental setup of graphite mixed EDM (a) photographic view (b) schematic view

2.3. Selection of input parameters and responses

The machining characteristics are largely affected by several electrical and powder related input parameters. In this particular experiment, five input parameters were selected with three levels out of which, three were electrical and two were powder related parameters. The parameters are current (I), pulse on time (P_{on}), duty cycle (DC), powder concentration (C_p) and mesh size (m). Based on the machining capacity and availability of powders, the minimum, intermediate and maximum level of each input parameter were chosen. Table 4 represents the input parameters and their levels. Box- Behnken Design (BBD) of response surface methodology (RSM) was used to construct the plan of experiments. The BBD design provides a high order quadratic model with small number of experimental run compared to other design of the RSM model. According to the scheme of BBD design, the number of experimental runs consist only the midpoints of the cube edges. No center points and axis points are present in it like central composite design or other models [31]. Along with that, the variance of the model is uniform in design space. For 5 factor BBD design, total 40 edge points and 6 center points have been considered and the L46 array of design has been

developed. The MINITAB 17 software has been used to construct the experimental table.

Table 4. Input parameters with their levels.

Input Parameter	Unit	Low level	Intermediate Level	High Level
Current (I)	A	4	8	12
Pulse on time (P_{on})	µs	35	55	75
Duty Cycle (DC)		0.5	0.7	0.9
Powder concentration (C_p)	g/l	2	5	8
Mesh Size (m)	µm	15	25	35

After the experiment, three responses were measured for each sample and listed their values in Table 5; they are the material removal rate (MRR), surface roughness (SR) and tool wear rate (TWR). MRR represents the productivity of the machining which is determined by measuring the volume of material removal per unit time.TWR represents the consumption of electrode which is measured as the amount of tool eroded per unit time while machining. In this study, the MRR and TWR were measured using Eq. 1 and Eq. 2 respectively and expressed in terms of mm^3/min. The SR is the vertical unevenness of the machined surface measured from a mean line. SR relates the quality of machining and the texture of the newly developed surface. The center line average (CLA) or R_a surface roughness was measured in this study by a stylus type precision profilometer (model name: Talyor Hobson, Surtronic 3+). In each surface, three measurements were taken and the mean value of the measurements was listed in Table 5. Atomic force microscopy (AFM) was also used to measure the precise value of surface roughness of three samples machined at three different levels of current.

$$MR = \frac{\frac{Difference\ of\ mass\ of\ the\ workpiece\ before\ and\ after\ machining \times 1000}{machining\ time \times density\ of\ work\ material}}{} \quad (1)$$

$$TWR = \frac{\frac{Difference\ of\ mass\ of\ the\ tool\ before\ and\ after\ machining \times 1000}{machinig\ time \times density\ of\ tool\ material}}{} \quad (2)$$

In this study, the density of Inconel 625 was taken as 8.44 g/cm^3 and density of the copper was taken as 8.83 g/cm^3. The machining time for each sample was kept constant at 15 minutes.

2.4. RSM modeling and Multi response optimization

Response surface methodology (RSM) was introduced by Box and Wilson on 1951. It is used mainly to optimize different manufacturing, production and chemical processes. The approach of RSM is initiated with developing an experimental design consideringinput parameters and their levels. Further, the experiments are conducted using the design and the responses are measured. The RSM analysis provides a quadratic mathematical model which consists the linear, square and interaction terms of the input parameters and develops a second order regression equation as shown in Eq. 3 [32].Beside the equation, it generates response surfaces with contour plots over the interaction plane of two input parameters. The response surface determines the effect of input parameters and their interactions on responses. Beside this, the quadratic model helps to predict data at different combination of input parameters other than the experimental run.

$$Y = \beta_0 + \sum_{i=1}^{5} \beta_i\, x_i + \sum_{i=1}^{5} \beta_{ii}\, x_{ii}^2 + \sum_{i=1}^{5} \sum_{j=1\ (j \neq i)}^{4} \beta_{ij}\, x_i x_j + \varepsilon \quad (3)$$

In this equation, Y is response, β_0 is the fitted value of the centre point response, β_i, β_{ii}, β_{ij} are the coefficients of linear, quadratic and interaction terms of the regression, x_i, x_j are coded input parameters and ε is the error coupled with the model.

Multi response optimization is another mathematical technique which derives the optimal solution of the responses for a particular set of values of the input parameters. It is done based on the multiple desired goal of responses imposed in the model. RSM is one of the simple mathematical approach which does not require any complicated equation. In this study, desirability function approach is used by conjugating three objectives such that the optimization provides maximum MRR, minimum TWR and minimum SR. Initially, a desirability function $d_i(y_i)$ is derived from the regression equation y_i for each response. Eq. 4 and Eq. 5 depict two methods to calculate desirability function when the optimization is performed between the minimum and maximum value of the regression equation. In Eq. 4, $d_i(y_i)$ is calculated when the response is to be maximized. However, to minimize the response, Eq. 5 is used. In both the equations, U_i and $L_i$represent the upper and lower value of ith regression equation. Further, if a response is to optimize at a target value, the U_i for maximization and L_i for minimization will be replaced by target value (T_i). In this way, the desirability functions generated from the individual responses are then simply multiplied to obtain composite desirability function (D) as shown in the Eq. 6. Further, D is maximized and the optimal result is obtained.

$$d_i(y_i) = \frac{y_i - L_i}{U_i - L_i} \quad (4)$$

$$d_i(y_i) = \frac{y_i - U_i}{L_i - U_i} \quad (5)$$

$$D = \left(\prod_{i=1}^{n} d(y_i)\right)^{1/n} \quad (6)$$

Presently, y_i is the regression equation of ith response, and $d(y_i)$ is the desirability function of it. D is the overall desirability function. n is the number of responses.

2.5. Mathematical model using artificial neural network

Artificial neural network (ANN) is a part of deep learning process used to predict an output after a rigorous training of similar type data. The basic structure of neural network was constructed based on the human nervous system. Like the main unit of the nervous system, this network also consists of several neurons connecting to other set of neurons with a mathematical relationship [33]. The scheme of the ANN model is shown in Fig. 2.In this model, the circles represent the neurons and they are connected by the straight lines called synapses. The synapses are assigned by a weight factor. One neurons receive signal from other neuron by multiplying the signal weight factor. The network consists at least three layers viz. one input layer, one output layers and on hidden layer. However, multiple hidden layers may be used based on the requirement of the model. For the requirement of the present study, a three layer neural network has been constructed where the input layers and output layer consist 5 and 3 neurons respectively. Since a very large and too small number of neurons reduce the accuracy of prediction, the hidden layer has been constructed with 20 neurons. This number has been considered after making several trials.

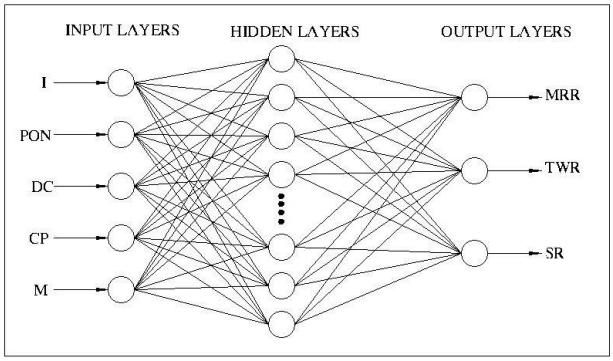

Figure 2. Three layer based neural network for predicting the responses

ANN is basically a statistical and mathematical model where the responses are predicted after several training of the model with an experimental data set [33]. In this method, a set of data point for each input parameter is assigned in the neurons of input layers. Now the values (also called signal) are transferred to the next layer by multiplying the weight factor allotted by the model itself. Each neuron of the hidden layer receives the input as a sum of the weighted signal coming from every neuron of input layer. Further, the signal received by the neuron of hidden layer is activated by an activating function and transferred to next layer (output layer in this case) again by multiplying a weight factor. Finally, the neuron of the output layer generates the predicted response by converting the received signal in to output training function. It is quite obvious the output signals will not match with the actual values of responses. Hence, the mean square error (MSE) is calculated between actual and predicted. If the error is found large, the feedback will be received by the network and it changes the weight factor in each synapse and repeat the training process further. This complete cycle consisted of training of the network, MSE measurement, feedback generation and backpropagation is called an epoch. The network is performing its computation till it reaches the specified number of epoch or a value of MSE whichever is achieved earlier. Six activation functions viz. Hyperbolic tangent sigmoid function, denoted (tansig) Log-sigmoid function, denoted by (logsig), Linear function (purelin), Positive linear function (rectilin), Conjugate gradient with Polak-Ribiére (CGP) and One-step secant (OSS) are commonly used in hidden layers. However, the selection of activation function solely depends on the nature of problem, non-linear complex relationship between input and output and the number of data point [34].

The accuracy of the network is measured by calculating the mean error followed by percentage relative error between actual data and the predicted data. During the network modeling, 2/3rd of the total experimental data were selected as training data and 1/3rddata were further tested by it [35]. Testing is performed with the remaining data after completion of training and the predicted result was compared with the actual data. The relative error was calculated by Eq. 7 and the mean error is calculated by Eq. 8.

$$\%Relative\ error = \frac{(actual\ data - predicted\ data)\times 100}{actual\ data} \quad (7)$$

$$Mean\ error = \frac{\sum \%\ relative\ error}{number\ of\ data\ point} \quad (8)$$

3. Result and Analysis

The result of the present experiment has been presented in Table 5 by enlisting the measured values of all the three responses. From the Table 5, it can be observed that the maximum values of MRR, TWR and SR are 30.772 mm^3/min, 0.2039 mm^3/min and 12.33 µm respectively whereas the minimum values are 2.204 mm^3/min, 0.0129 mm^3/min and 3.12 µm respectively. The main aspects of this discussion are limited to parametric analysis, accuracy of the ANN model, multi objective optimization using desirability function and surface characterization.

3.1. Analysis of responses

3.1.1. Effect on MRR

Material removal rate (MRR) is one of the important parameter to measure the machinability of a process as it is directly proportional to the rate of productivity. In industrial application, MRR needs to be maximized to enhance the production. In the Fig. 3(a), the variations of MRR are shown against their mean values with respect to the input parameters. It can be observed the MRR varies notably with current, powder concentration and mesh size. Also in the Fig. 3(a),the variation of MRR is found maximum in case of change in current from lower to higher level. From Table 5, the average of MRR values for lower, intermediate and higher level can be calculated as 4.732 mm^3/min, 18.379 mm^3/min and 27.217 mm^3/min respectively. However, it is found that the enhancement from low level to intermediate level with respect to intermediate level is 74.25% and intermediate level to high level with respect to intermediate level is 48.08%. It indicates the rate of enhancement is higher for changing the current from lower to intermediate compare to the changing of current between intermediate to higher level. The principal reason of increasing MRR is the enhancement of energy transfer rate on the surface. Material is melted and vaporized at a higher rate due to the high energy transfer. Now, high energy transfer occurs mainly due to increase of the current which directly provides more energy to the discharges. On the other hand, the increase of concentration adds more graphite particle in dielectric. The concentrated graphite particles thus emits more local discharges and utilize the spark energy uniformly over the machining surface.Along with this, increase of graphite concentration in the dielectric fluid increases the electrical conductivity of the solution. Graphite particles are arranged in a chain from electrode to workpiece surface at different locations which provides a varying conductivity over the machining region and creates additional discharges from each chain. With the increase of graphite particles the number of chains and thus conductivity increase which lead to the enhancement of discharges. As a result, the removal of material increases compared to the removal rate at lower powder concentration. The mesh size of the graphite particles plays an interesting role in changing of MRR. In the Fig. 3(a), it can be seen that the MRR decreases when mesh size increases from 15 µm to 25µm and increases slightly till 35 µm. The rate of mixing with dielectric for small particles are better than large particles. Therefore the small particles can effectively take part on local discharging compared to large particles and removes materials from the surfaces. However a little large particle can induce and discharge high energy spark as it has high surface area. Therefore, the MRR increases slightly when the mesh size changes from25 µm to 35 µm.

Table 5. Experimental result for MRR, TWR and SR.

Run no.	Current	Pulse on Time	Duty Cycle	Powder Concentration	Powder mesh size	MRR	TWR	SR
	(A)	(µs)		(g/l)	(µm)	(mm^3/min)	(mm^3/min)	(µm)
1	8	55	0.7	5	25	16.659	0.0797	9.08
2	8	75	0.5	5	25	18.780	0.0810	9.99
3	12	55	0.7	5	35	29.068	0.1627	8.50
4	8	55	0.9	5	35	20.468	0.0882	8.34
5	8	55	0.7	2	35	16.736	0.0574	10.32
6	8	55	0.7	5	25	18.602	0.0763	8.86
7	8	35	0.7	8	25	16.563	0.0680	7.41
8	4	55	0.7	8	25	3.989	0.0190	4.67
9	12	35	0.7	5	25	28.919	0.1493	12.33
10	12	55	0.7	8	25	29.452	0.1419	9.11
11	8	75	0.9	5	25	15.450	0.0921	9.08
12	8	55	0.7	2	15	19.879	0.0863	8.69
13	12	75	0.7	5	25	27.923	0.1654	10.39
14	8	55	0.9	2	25	16.983	0.0762	8.69
15	8	55	0.7	8	15	23.324	0.0664	9.58
16	8	55	0.9	5	15	21.771	0.0782	8.46
17	12	55	0.7	5	15	30.772	0.1656	11.56
18	8	35	0.5	5	25	12.994	0.0861	8.74
19	4	55	0.9	5	25	4.404	0.0157	4.20
20	8	35	0.7	5	15	14.739	0.0881	9.53
21	8	55	0.5	8	25	20.468	0.0728	8.29
22	8	55	0.7	5	25	18.697	0.0991	6.72
23	12	55	0.5	5	25	23.697	0.1738	11.62
24	8	75	0.7	5	15	27.921	0.0685	9.55
25	4	55	0.7	5	35	4.333	0.0249	3.12
26	4	55	0.5	5	25	4.542	0.0132	4.10
27	8	55	0.7	5	25	20.024	0.0823	7.58
28	8	35	0.9	5	25	13.586	0.0813	9.57
29	8	55	0.9	8	25	23.726	0.0775	7.13
30	8	55	0.5	5	15	19.431	0.0650	10.79
31	12	55	0.7	2	25	20.472	0.2039	10.93
32	8	55	0.5	5	35	16.055	0.0998	6.74
33	8	75	0.7	2	25	17.546	0.0789	9.86
34	8	55	0.5	2	25	12.576	0.0737	10.98
35	8	55	0.7	8	35	20.438	0.0642	7.81
36	8	75	0.7	8	25	20.201	0.0781	7.43
37	8	35	0.7	2	25	15.521	0.0991	8.28
38	4	55	0.7	2	25	6.536	0.0884	6.12
39	8	55	0.7	5	25	16.543	0.0944	10.14
40	4	35	0.7	5	25	2.204	0.0159	4.60
41	8	55	0.7	5	25	19.589	0.0775	8.66
42	4	75	0.7	5	25	7.701	0.0261	4.53
43	4	55	0.7	5	15	4.147	0.0129	3.92
44	12	55	0.9	5	25	27.429	0.1886	10.76
45	8	75	0.7	5	35	8.672	0.0713	10.14
46	8	35	0.7	5	35	27.429	0.0827	7.90

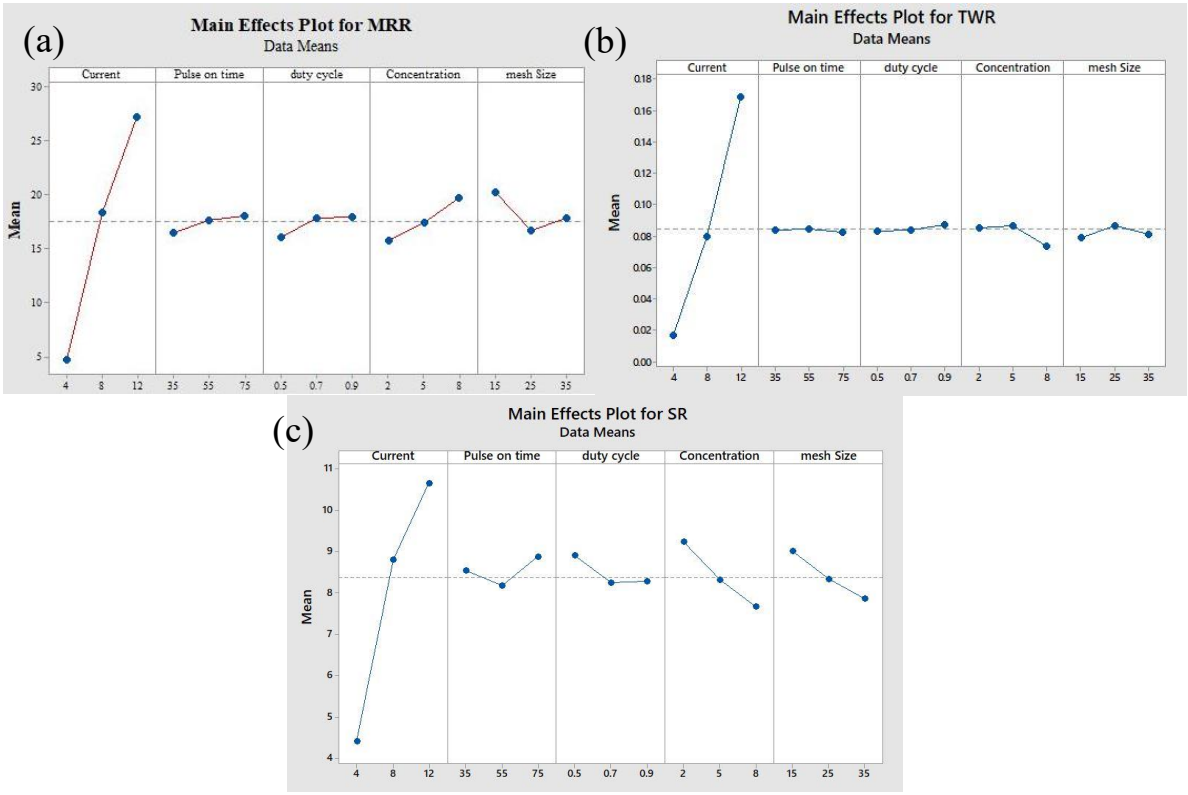

Figure 3. Main effect plot of (a) MRR (b) TWR and (c) SR

3.1.2. Effect on TWR

Tool wear rate (TWR) is directly related to the consumables required for the machining. In mass scale production, the aim of the machining should be reducing the tool wear. In EDM, tool or electrode has high thermal conductivity so that the temperature of the tool surface must not increase significantly. The tool wear phenomenon is associated with the removal of the metal from the surface of tool. In EDM, the tool wear occurs due to the melting and vapourization of the tiny material from the tool electrode due to the rise of temperature beyond the melting point at certain portions of the surface. The transfer of thermal energy is the main reason behind the increase of temperature of the surface. When the electrode is discharging and electrons are flowing through the plasma channels, the positive ions are moving opposite direction towards electrode surface and transfer heat energy on it. But the presence of graphite particles in the dielectric disrupts the movement of positive ions due to their zig zag motion during their discharges[36].The movement of particles and their discharges deflect the route of positive ions towards the surface and slowdowns the tool wear. In Fig. 3(b), it can be seen that TWR increases significantly with the increase of current. Whereasthe tool wear rate is constant with the increase of graphite powder concentration from 2 g/l to 5 g/l and decreased for 5 g/l to 8 g/l.This phenomenon can be explained as the disruption of positive ions are very low during the change of concentration from 2 g/l to 5 g/l and it is very high at 5 g/l to 8 g/l because more graphite particles enhance the disruption in better way. Along with that the increase of electrical conductivity with the increase of powder concentration induces more current in the plasma column. Due to which, the temperature of the tool surface increases and the tool wear rate increases. However, the conjugate action of these two phenomenon makes the TWR constant in the first section and lower down at the second section. The changes of tool wear for other three parameters are found less significant in this study. Like MRR, the variation of TWR is maximum in case of change in current from lower to higher level shown in the Fig. 3(b). From Table 5, the average of TWR values for lower, intermediate and higher level can be calculated as 0.0170 mm^3/min, 0.0800 mm^3/min and 0.1690 mm^3/min respectively. However, it is found that the enhancement from low level to intermediate level with respect to intermediate level is 78.65% and intermediate level to high level with respect to intermediate level is 111.99%. Unlike MRR, it indicates that the rate of enhancement is lesser for changing the current from lower to intermediate compare to the changing of current between intermediate to higher level.

3.1.3. Effect on SR

The quality of surface generated during machining is one of the important criterion for the quality production. It is quite normal that the surface roughness increases with increase of MRR. In EDM, the surface is generated by melting and vaporization of the material. When the materials melts and removes from surface, it leaves a small concave shaped crater on the surface. Moreover, the melted material further deposits on the freshly generated surface in the form of recast layer and the distribution of this layer is not uniform. These are two major reasons of getting high surface roughness. In the Fig.3(c), the variation of surface roughness SR has been shown with respect to the increase of input parameters. The major influences have been investigated for current, powder concentration and powder mesh size. SR remarkably increases with increase of current but decreases with graphite concentration and graphite mesh size. The increase of current removes the material at a faster rate which increases the crater depth by removing more material from a particular area. This contributes to enhance the peak to valley distance of a particular point. Whereas the high concentration of graphite powder distributes the spark uniformly over the surface. This increases the number of spark at the different region of the

cutting surface. Due to which, more number of craters are generated in unit areas due to removal of material. The craters get overlapped as their density in the unit area increase which leads to reduce their depth and inside unevenness. The reduction in crate depth and unevenness therefore reflected on the surface roughness to reduce. However, large mesh size reduces the energy density of the particles at the discharged region. Due to these, the craters on the machined surface get shallower compared to the discharge of small meshed graphite particle. This leads to a reduction in surface roughness observed on the sample after the machining. The pulse on time and duty cycle has less effect on surface roughness. Normally surface roughness increases with increase of pulse on time as higher pulse time increases the crater depth. The increase of duty cycle promotes the sufficient flushing timefor removed material which prevents the formation of recast layer for which surface roughness decreases. Refer to Fig. 3 (c), The variation of SR is found maximum in case of change in current from lower to higher level shown like MRR and TWR. From Table 5, the average of SR values for lower, intermediate and higher level can be calculated as 4.407 µm, 8.811 µm and 10.650 µm respectively. However, it is found that the enhancement from low level to intermediate level with respect to intermediate level is 49.97% and intermediate level to high level with respect to intermediate level is 20.86%. The result indicates the rate of enhancement is higher for changing the current from lower to intermediate compare to the changing of current between intermediate to higher level.

3.2. ANOVA and Regression analysis

3.2.1. ANOVA

A brief idea regarding the significance of each input parameter is already achieved in main effect plots shown in Fig. 3. However, the significance of each input parameter, their contribution and the model fitness can be calculated statistically by analysis of variance method (ANOVA). In the calculation of ANOVA, adjusted sum of square, mean square, F value and P value of each parameter and their interaction terms are calculated. Along with that the percentage contribution of each significant parameter on the response has been calculated as the ratio of adjusted sum of square of that parameter to the total adjusted sum of square of all the components of ANOVA. Table 6 represents the ANOVA result calculated for MRR with 95% confidence level. In the analysis, the p values for current, powder concentration, mesh size, square term of the current and mesh size and interaction term of current with pulse on time and pulse on time with mesh size are found less than 0.05. Hence, the contribution of these terms are significant to change the responses. The contribution of current, powder concentration and mesh size are 75.55%, 2.38% and 0.82% respectively. It is observed that pulse on time is an insignificant parameter but interacting with current and mesh size it changes the responses significantly as the latter two terms are highly significant. Table 7 represents the ANOVA of tool wear rate. In this analysis, the significant terms are found current, powder concentration, square of the current term and interaction of current and powder concentration. The percentage contributions of current and powder concentration are 92.90% and 0.57% respectively. In case of surface roughness, the ANOVA result is shown in Table 8. The significant terms are found current, powder concentration and mesh size and the square of current. The contribution of the significant terms are 68.11%, 4.22% and 2.31% respectively. From the ANOVA of three responses, it is clear that current and powder concentration as are the most influential parameters responsible to vary all the three responses. Also, the p value of model and lack of fit for three responses are found less than 0.05 and greater than 0.05 respectively which indicate the models are significant and fitting of quadratic polynomial in these data is accepted [37]. The other terms having >0.05 value of p are insignificant for all the three responses.

Table 6. ANOVA result for MRR

Sl no.	DOF	Adj SS	Adj MS	F Value	p Value
Model	20	2555.29	127.76	26.36	0.000*
I	1	2022.21	2022.21	417.20	0.000*
P_{on}	1	9.36	9.36	1.93	0.177
DC	1	14.58	14.58	3.01	0.095
C_p	1	63.65	63.65	13.13	0.001*
M	1	22.05	22.05	4.55	0.043*
I^2	1	50.05	50.05	10.33	0.004*
P_{on}^2	1	4.05	4.05	0.84	0.369
DC^2	1	8.68	8.68	1.79	0.193
C_p^2	1	0.00	0.00	0.00	0.993
M^2	1	26.37	26.37	5.44	0.028*
$I \times P_{on}$	1	10.54	10.54	2.17	0.153
$I \times DC$	1	3.74	3.74	0.77	0.388
$I \times C_p$	1	33.22	33.22	6.85	0.015*
$I \times M$	1	0.89	0.89	0.18	0.671
$P_{on} \times DC$	1	3.85	3.85	0.79	0.382
$P_{on} \times C_p$	1	0.65	0.65	0.13	0.717
$P_{on} \times M$	1	255.02	255.02	52.61	0.000*
$DC \times C_p$	1	0.33	0.33	0.07	0.796
$DC \times M$	1	1.07	1.07	0.22	0.642
$C_p \times M$	1	0.02	0.02	0.00	0.954
Lack of Fit	20	110.53	5.53	2.60	0.147
Pure Error	5	10.65	2.13		
Total	45	2676.46			

$R^2 = 0.9547$ R^2 Adjusted = 0.9185 R^2 Predicted = 0.8291

Table 7. ANOVA result for TWR

Sl no.	DOF	Adj SS	Adj MS	F Value	p Value
Model	20	0.097519	0.004876	40.22	0.000*
I	1	0.092952	0.092952	761.23	0.000*
P_{on}	1	0.000005	0.000005	0.04	0.838
DC	1	0.000066	0.000066	0.54	0.469
C_p	1	0.000576	0.000576	4.75	0.039*
M	1	0.000026	0.000026	0.21	0.650
I^2	1	0.001120	0.001120	9.24	0.005*
P_{on}^2	1	0.000023	0.000023	0.19	0.667
DC^2	1	0.000384	0.000384	0.07	0.793
C_p^2	1	0.000384	0.000384	3.16	0.087
M^2	1	0.000290	0.000290	2.39	0.135
$I \times P_{on}$	1	0.000009	0.000009	0.07	0.791
$I \times DC$	1	0.000038	0.000038	0.31	0.581
$I \times C_p$	1	0.001318	0.001318	10.87	0.003*
$I \times M$	1	0.000056	0.000056	0.46	0.505
$P_{on} \times DC$	1	0.000063	0.000063	0.52	0.477
$P_{on} \times C_p$	1	0.000230	0.000230	1.89	0.181
$P_{on} \times M$	1	0.000017	0.000017	0.14	0.713
$DC \times C_p$	1	0.000001	0.000001	0.01	0.921
$DC \times M$	1	0.000154	0.000154	1.27	0.271
$C_p \times M$	1	0.000178	0.000178	1.47	0.237
Lack of Fit	20	0.002576	0.000129	1.42	0.374
Pure Error	5	0.000454	0.000091		
Total	45	0.100549			

$R^2 = 0.9699$ R^2 Adjusted = 0.9457 R^2 Predicted = 0.8910

Table 8. ANOVA result for SR

Sl no.	DOF	Adj SS	Adj MS	F Value	p Value
Model	20	203.839	10.192	10.20	0.000
I	1	155.875	155.875	155.94	0.000*
P_{on}	1	0.426	0.426	0.43	0.520
DC	1	1.575	1.575	1.58	0.221
C_p	1	9.672	9.672	9.68	0.005*
M	1	5.303	5.303	5.30	0.030*
I^2	1	11.913	11.913	11.92	0.002*
P_{on}^2	1	1.426	1.426	1.43	0.244
DC^2	1	0.545	0.545	0.55	0.467
C_p^2	1	0.041	0.041	0.04	0.842
M^2	1	0.013	0.013	0.01	0.909
I × P_{on}	1	0.874	0.874	0.87	0.359
I × DC	1	0.230	0.230	0.23	0.635
I × C_p	1	0.034	0.034	0.03	0.855
I × M	1	1.277	1.277	1.28	0.269
P_{on} × DC	1	0.757	0.757	0.76	0.392
P_{on} × C_p	1	0.608	0.608	0.61	0.443
P_{on} × M	1	1.232	1.232	1.23	0.277
DC × C_p	1	0.319	0.319	0.32	0.577
DC × M	1	3.861	3.861	3.86	0.061
C_p × M	1	2.890	2.890	2.89	0.101
Lack of Fit	20	17.795	0.890	0.62	0.799
Pure Error	5	7.196	1.439		
Total	45	228.829			

R^2 = 0.8908 R^2 Adjusted = 0.8034 R^2 Predicted = 0.6437

3.2.2. Regression Equation

The result of the experiment is used to construct a second order equation using multivariable least square regression including all the interaction terms. Eq. 9, Eq. 10 and Eq. 11 represent the expression for MRR, TWR and SR respectively. The closeness of fitting of the data can be measured by the value of coefficient of determination (R^2). The R^2, R^2 adjusted and R^2 predicted data for MRR are 0.9547, 0.9185 and 0.8291 respectively. It indicates the closeness of fit with the model is quite satisfactory and the over fitting with each independent parameters are significantly less. Hence the model can be accepted. The same values for TWR are 0.9699, 0.9457 and 0.8910 respectively and the TWR model is found close to the experimental data. Also, the values of R^2, R^2 adjusted and R^2 predicted for SR are 0.8908, 0.8034 and 0.6437 respectively. In surface roughness the R^2 value is little less than 90% but the difference between adjusted R^2 and predicted $R^2$is less than 0.2. Hence the adequacy of the RSM model of SR is found very well and the overfitting of the data is within the range. Also, the experimental result for each experimental run have been compared with the value generated by regression equation and shown in Fig. 4. In Fig. 4 (a)-(c), the experimental result of MRR, TWR and SR have been plotted against the regression value respectively.

$$MRR = -80.3 + 4.57\,I + 1.524\,P_{on} + 39.4\,DC - 1.35\,C_p + 1.112\,\mathrm{M} - 0.1497\,I^2 - 0.0017\,P_{on}^2 - 24.9\,DC^2 + 0.0008\,C_p^2 + 0.01738\,M^2 - 0.0203\,I \times P_{on} + 1.21\,I \times DC + 0.2401\,I \times C_p - 0.0118\,I \times M - 0.245\,P_{on} \times DC + 0.0067\,P_{on} \times C_p - 0.03992\,P_{on} \times M - 0.48\,DC \times C_P + 0.259\,DC \times M + 0.0021\,C_p \times M \quad (9)$$

$$TWR = -0.061 + 0.01384\,I - 0.00131\,P_{on} - 0.037\,DC + 0.0043\,C_p + 0.00425\,\mathrm{M} + 0.000708\,I^2 - 0.000004\,P_{on}^2 + 0.0247\,DC^2 - 0.000737\,C_p^2 - 0.000058\,M^2 + 0.000018\,I \times P_{on} + 0.00384\,I \times DC - 0.001513\,I \times C_p - 0.000093\,I \times M + 0.00099\,P_{on} \times DC + 0.000126\,P_{on} \times C_p + 0.000010\,P_{on} \times M + 0.00092\,DC \times C_P - 0.00310\,DC \times M + 0.000222\,C_p \times M \quad (10)$$

$$SR = 4.7 + 2.872\,I - 0.017\,P_{on} - 16.6\,DC + 0.463\,C_p - 0.319\,\mathrm{M} - 0.073\,I^2 + 0.001010\,P_{on}^2 + 6.25DC^2 + 0.0076\,C_p^2 + 0.00039\,M^2 - 0.00584\,I \times P_{on} - 0.3\,I \times DC - 0.0077\,I \times C_p - 0.0141\,I \times M - 0.109\,P_{on} \times DC - 0.00650\,P_{on} \times C_p + 0.00277\,P_{on} \times M + 0.471\,DC \times C_P + 0.491\,DC \times M - 0.0283\,C_p \times M \quad (11)$$

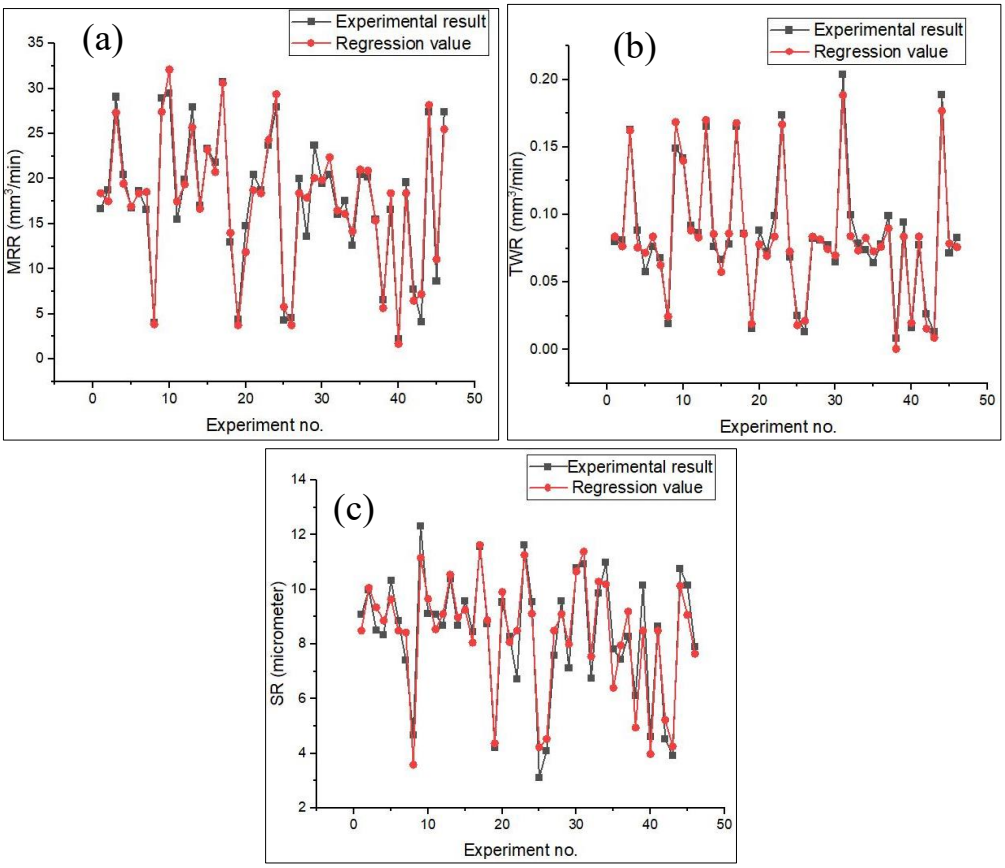

Figure 4. Comparison of experimental result with regression value (a) MRR (b) TWR and (c) SR

The normal probability plot measures the distribution of the residual points along the normal probability line. In Fig. 5 (a), 5 (b) and 5 (c), it can be observedthat the residual points of MRR, TWR and SR are situated close to the probability line. Hence, it can be stated that the residuals are distributed normally and confirms that the fitness of the quadratic models are adequate.

3.3. Response surfaces against the interaction of two parameters

From the ANOVA result of the three responses, it has already been revealed that the two major significant parameters for this investigation are current and powder concentration. Hence 3D response surfaces can be generated for each of the three responses considering the interaction of two input parameters. The surfaces are generated using DESIGN EXPERT 12 software. Fig. 6(a) shows the interaction plot of MRR which indicates that the maximum MRR can be achieved when current is at 12 A and powder concentration is 8 g/l. Since MRR is increasing with increase of both current and graphite concentration, the maximum value can be achieved at the maximum value of both the parameters. In Fig. 6(b), the surface plot of TWR is represented which conveys the minimum TWR can be achieved when the current is 4 A and the powder concentration is 8 g/l. It is already proved that at low current and high graphite concentration, the flow of positive ions toward electrode decelerates and disrupts. As a consequence, the minimum TWR is achieved at the above said values. In Fig. 6(c), the nature of the surface plot is slightly different than other two responses. A convex type surface plot is achieved where the lowest surface roughness is found at a current of 4 A and powder concentration of 8 g/l. At the low current discharge, the depth of the crater becomes small due to the removal of small size material from the surface. Also at high powder concentration, more local discharges take place which produce uniform and shallow craters in the discharge region. The combine effect of these two parameters at their aforesaid level values, however, produces the least surface roughness.

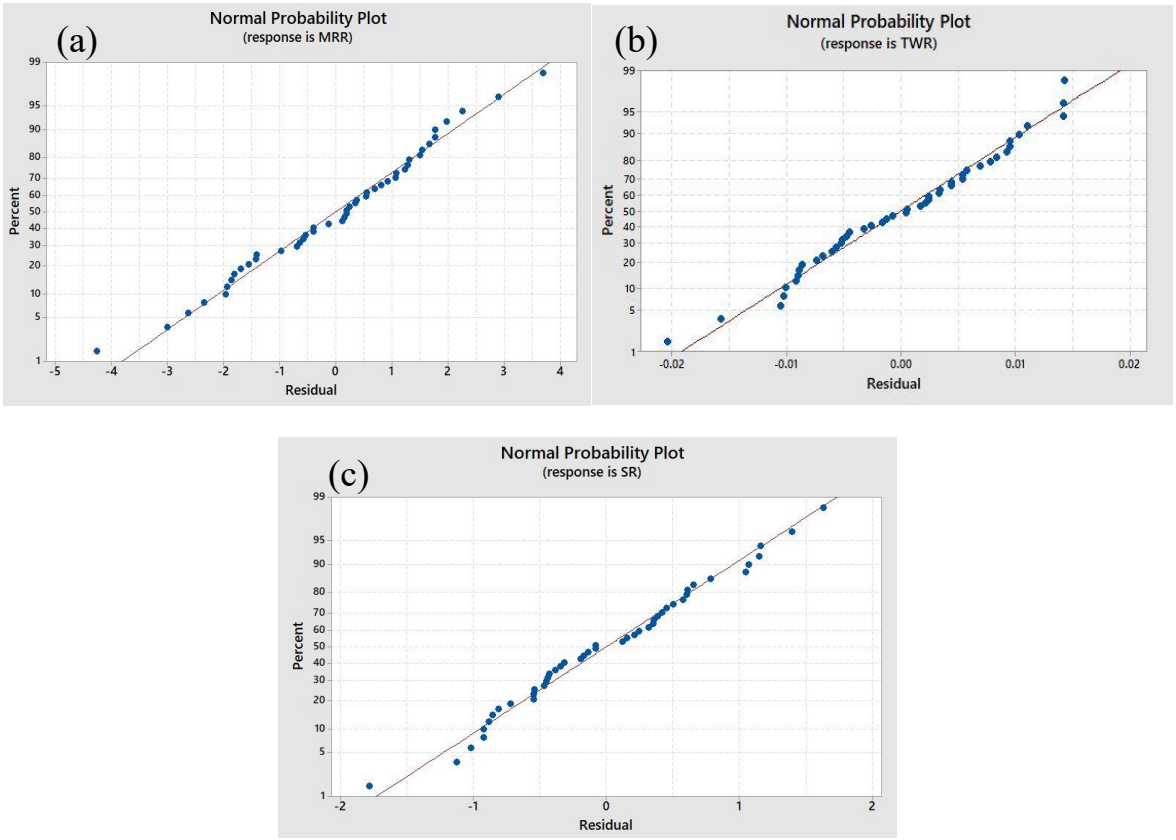

Figure 5. Normal probability plot of (a) MRR (b) TWR and (c) SR

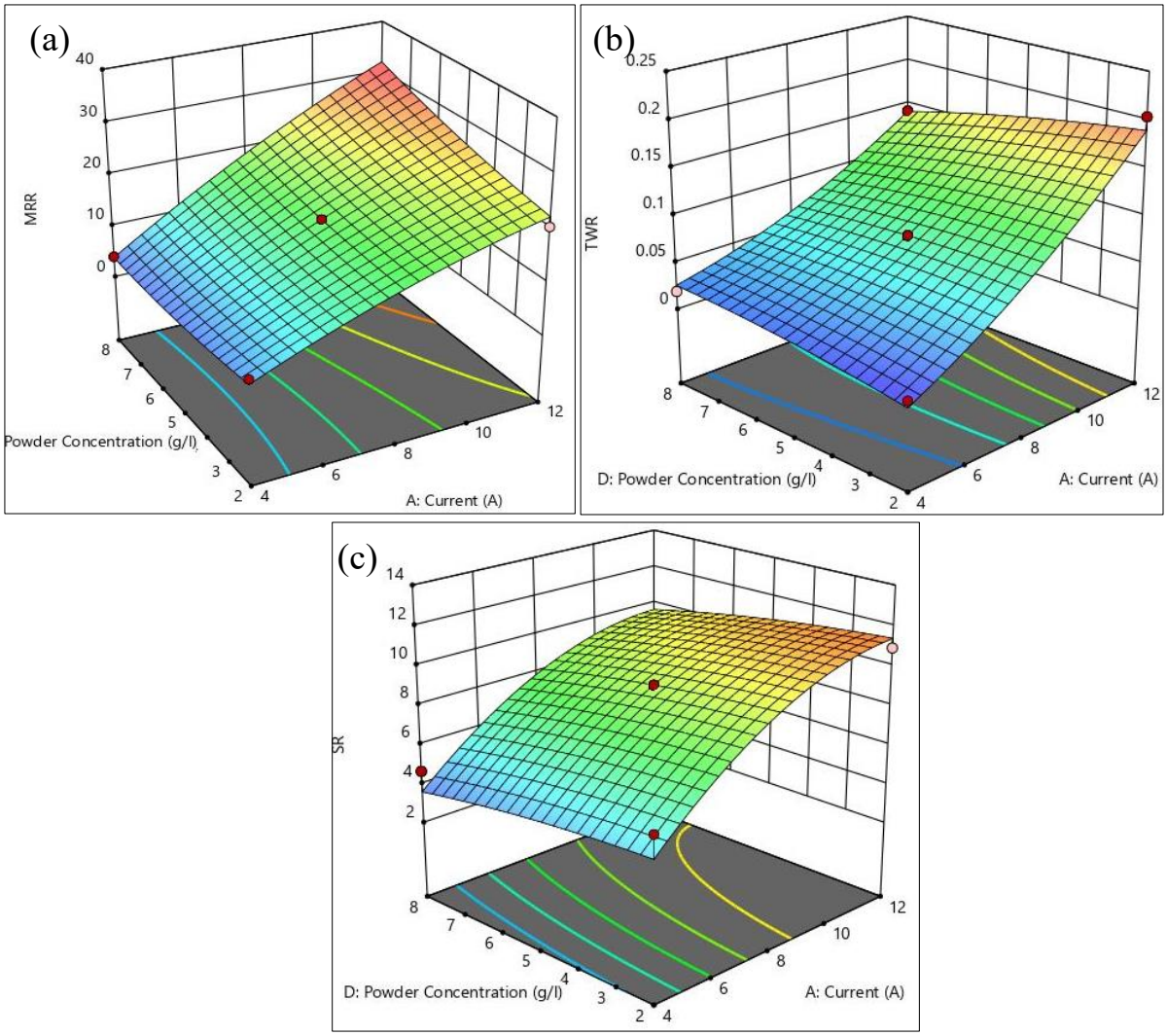

Figure 6. 3D surface plot for (a) MRR (b) TWR and (c) SR against the interaction of current and powder concentration

3.4. ANN Result

In the present study, a 5-20-3 neural network has beendeveloped using neural network toolbox in MATLAB R2021 a. It is a feed forward backpropagation type networkwhere the training function, learning function and performance function are chosen as TRAINLM, LEARNGOM and MSE respectively. After several trials made by different combination of network, a single hidden layer with 20 neurons has beenselected for this analysis. The activation functions for the hidden layer and the output layerwereselected as hyperbolic tangent sigmoid function (Tansig) and pure linear function (Purelin) respectively. In several researches, it has been found that the effect of performance parameters on the responses during EDM is highly nonlinear [38]. In ANN, the nonlinear interaction between hidden layers can be efficiently performed by a nonlinear sigmoid function. During the training of network, the stopping criterion was set as 1000 epochs or an error of 0 whichever reaches earlier. During the training of the network, arbitrarily 30 results were chosen for training of the network. The remaining 16 results were kept for testing the data. After completion of the training, the testing dataset was simulated with trained network and the predicted result was generated.

In table 9, the prediction of the training and testing results have been provided. In the table, the experimental result and the predicted result are compared for all the three responses. A percentage relative error is calculated for every prediction. In the table, it can be observed that the percentage relative error has a wide range for different runs and different responses. However, a mean error has been calculated according to Eq. 8 considering all the 46 predictions. The mean error for MRR, TWR and SR is 5.95%, 7.30% and 6.40% respectively. The mean error for all the responses are found less than 10% which indicates the ANN model can predict the responses 90% closer to the actual result. In Fig. 7 (a)-(c), the prediction of the tested data are plotted against their experimental data for MRR, TWR and SR. In the graphical representation, red dots represent predicted data and black dots represent the actual data for all the three responses. It can be observed that the prediction lines and the lines made with actual values are situated closely even coincided somewhere. Fig. 8 shows the R-value (correlation coefficient) of training, validation, test and overall performance for the present neural network. Apart from test performance, the R-values of training and validation were found more than 0.9. The R-value of overall performance is 0.94509 which indicates the predicted values are distributed at close intervals with target data. In Fig. 9, the mean square error is plotted against the value of epoch. It is observed that the

training of the model has been completed with minimum error within 11 epochs. This indicates the training model takes less time of computation during the training.

In this study, two parameters related to the performance of neural network have been evaluated viz. mean error and R- value. In manufacturing industry, a new ANN model is adopted for production, machining and other work only when the values of these two parameters found closer to a standard one. In this study, the mean error and R values are found adequate to accept the model. With less than 10% mean error and R value as 0.94509, it can be well said that the model has a good correlation with experimental result and it can perform efficiently to predict the responses for the remaining combination of the input parameters in practice.

Table 9. Predicted result of MRR, TWR and SR using ANN.

Run No.	MRR			TWR			SR		
	Exp.	ANN pred.	%Error	Exp.	ANN pred.	%Error	Exp.	ANN pred.	%Error
Training data									
1	16.659	18.127	8.81	0.0797	0.0728	8.78	9.08	8.14	10.35
2	18.780	20.291	8.05	0.0810	0.0859	6.17	9.99	9.59	4.00
3	29.068	28.273	2.74	0.1627	0.1470	9.83	8.50	8.77	3.18
5	16.736	16.785	0.29	0.0574	0.0531	6.97	10.32	9.53	7.66
7	16.563	17.163	3.62	0.0680	0.0606	10.29	7.41	7.58	2.29
8	3.989	3.722	6.69	0.0190	0.0177	5.26	4.67	4.55	2.57
9	28.919	28.593	1.13	0.1493	0.1412	5.36	12.33	11.46	7.06
11	15.450	14.202	8.08	0.0921	0.0500	45.60	9.08	8.50	6.39
13	27.923	29.530	5.76	0.1654	0.1841	11.49	10.39	11.03	6.16
14	16.983	17.387	2.38	0.0762	0.0757	1.31	8.69	8.67	0.23
16	21.771	22.474	3.23	0.0782	0.0721	7.67	8.46	8.34	1.42
18	12.994	13.875	6.78	0.0861	0.0854	1.16	8.74	8.20	6.18
19	4.404	4.777	8.47	0.0157	0.0143	6.37	4.20	4.57	8.81
20	14.739	16.330	10.79	0.0881	0.0895	1.14	9.53	8.98	5.77
22	18.697	18.127	3.05	0.0991	0.0828	16.15	6.72	7.14	6.25
23	23.697	26.428	11.53	0.1738	0.1697	2.30	11.62	11.03	5.08
24	27.921	25.417	8.97	0.0685	0.0640	5.84	9.55	9.88	3.46
26	4.542	4.920	8.32	0.0132	0.0139	7.58	4.10	4.74	15.61
28	13.586	14.371	5.78	0.0813	0.0847	3.69	9.57	8.92	6.79
29	23.726	23.877	0.64	0.0775	0.0709	9.03	7.13	7.47	4.77
30	19.431	17.649	9.17	0.0650	0.0636	1.54	10.79	9.76	9.55
31	20.472	23.523	14.90	0.2039	0.2173	6.38	10.93	12.04	10.16
32	16.055	14.649	8.76	0.0998	0.0896	10.02	6.74	7.26	7.72
34	12.576	12.649	0.58	0.0737	0.0746	1.36	10.98	10.76	2.00
36	20.201	17.628	12.74	0.0781	0.0812	3.84	7.43	7.39	0.54
39	16.543	15.916	3.79	0.0944	0.0940	0.00	10.14	9.15	9.76
42	7.701	7.764	0.82	0.0261	0.0246	7.66	4.53	4.98	9.93
43	4.147	4.140	0.17	0.0129	0.0137	7.75	3.92	3.33	15.05
44	27.429	26.255	4.28	0.1886	0.1827	3.18	10.76	9.37	12.92
46	27.429	25.229	8.02	0.0827	0.0920	10.88	7.90	7.98	1.01
Testing data									
4	20.468	20.957	2.39	0.0882	0.0786	11.34	8.34	8.38	0.48
6	18.602	18.127	2.55	0.0763	0.0728	3.93	8.86	8.14	8.13
10	29.452	28.799	2.22	0.1419	0.1205	14.80	9.11	9.65	5.93
12	19.879	20.798	4.62	0.0863	0.0796	8.11	8.69	9.46	8.86
15	23.324	23.131	0.83	0.0664	0.0710	7.53	9.58	9.73	1.57
17	30.772	28.610	7.03	0.1656	0.1569	5.44	11.56	11.74	1.56
21	20.468	19.217	6.11	0.0728	0.0741	1.37	8.29	8.82	6.39
25	4.333	4.700	8.47	0.0249	0.0254	0.00	3.12	3.69	18.27
27	20.024	18.127	9.47	0.0823	0.0728	10.94	7.58	8.14	7.39
33	17.546	17.628	0.47	0.0789	0.0812	2.54	9.86	9.39	4.77
35	20.438	20.633	0.95	0.0642	0.0683	6.23	7.81	8.19	4.87
37	15.521	16.033	3.30	0.0991	0.0929	6.05	8.28	7.70	7.01
38	6.536	6.910	5.72	0.0884	0.0835	5.66	6.12	6.40	4.58
40	2.204	2.757	25.09	0.0159	0.0139	12.58	4.60	4.99	8.48
41	19.589	18.329	6.43	0.0775	0.0729	6.45	8.66	7.93	8.43
45	8.672	9.500	9.55	0.0713	0.0776	8.42	10.14	10.66	5.13

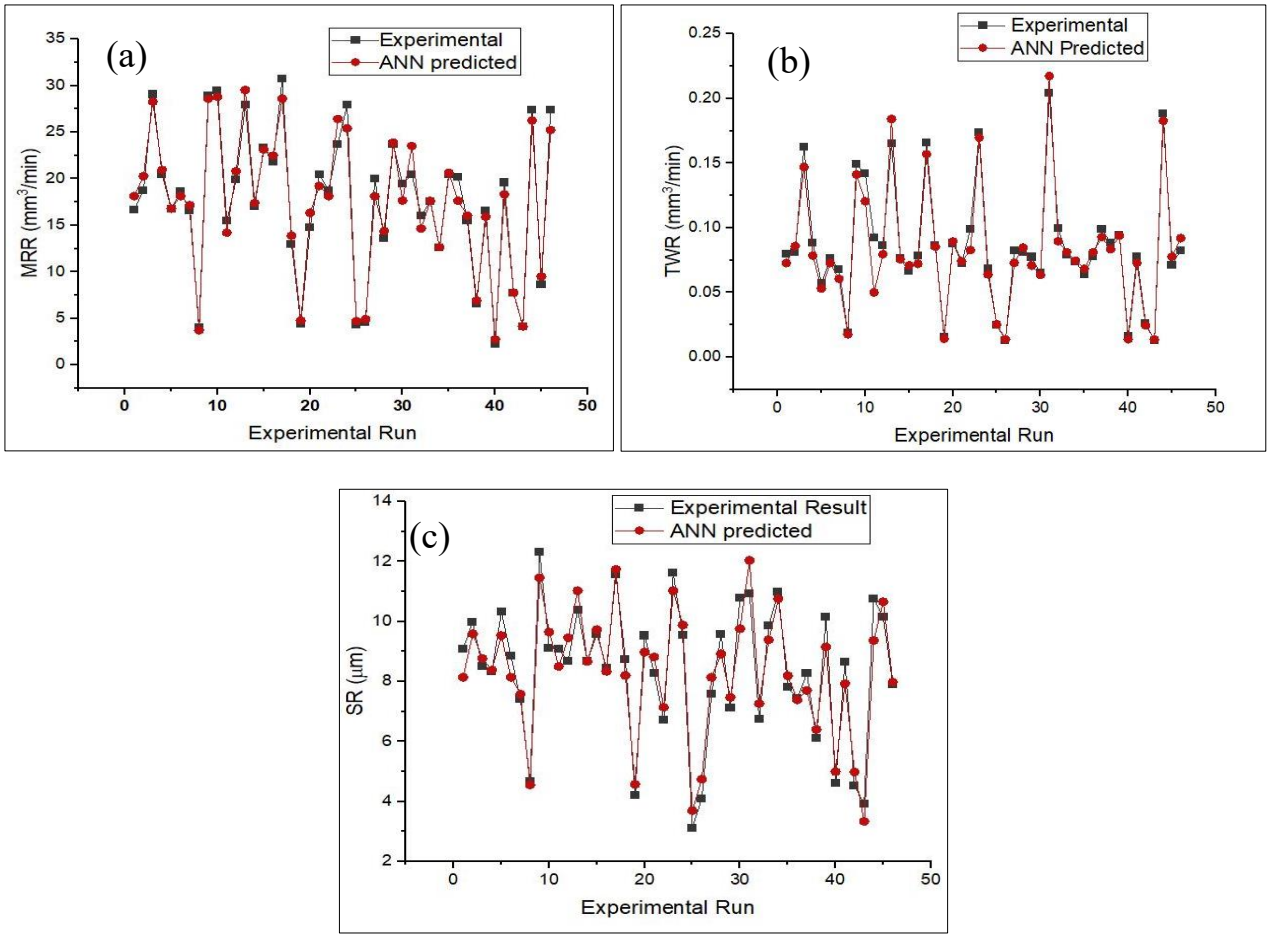

Figure 7. Comparison of ANN result and actual result for tested data of (a) MRR, (b) TWR and (c) SR

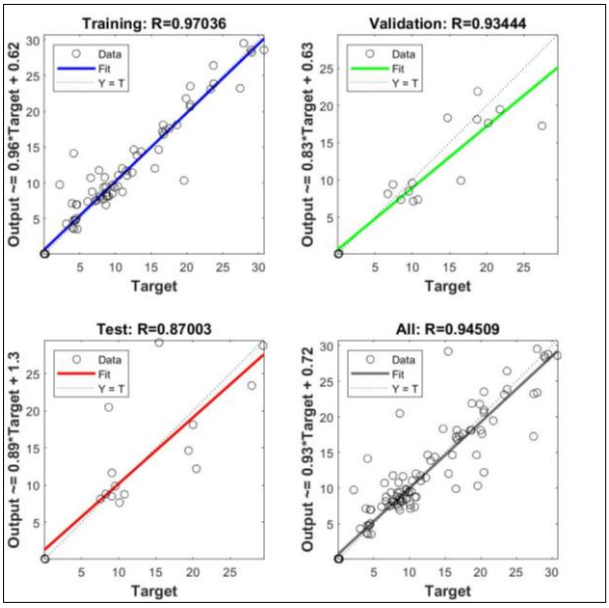

Figure 8. R- Values of the ANN model

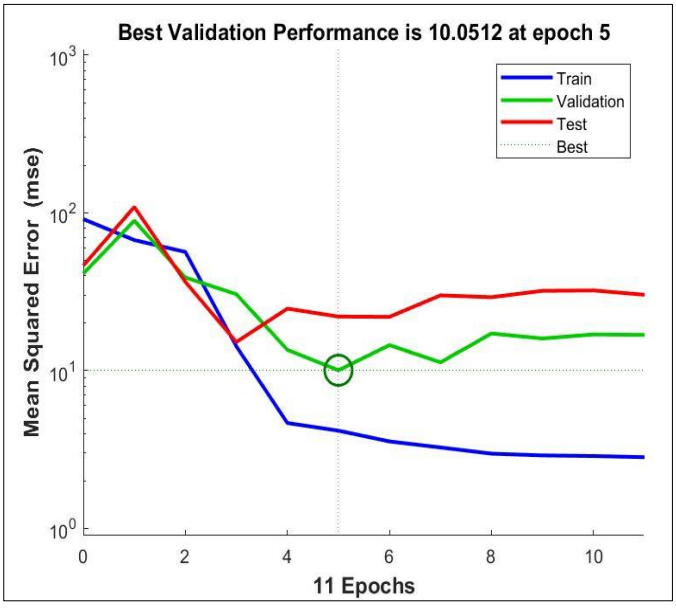

Figure 9. Epoch vs MSE plot during the training of the network

3.5. Multi response optimization using desirability function

In the present study, multi response optimization was performed using desirability function approach based on RSM equations. The objective functions were selected as to maximize MRR, minimize SR and to get a target value of TWR at 0.08 mm^3/min. The reason behind selecting a target level of TWR is to maximize MRR. In practical approach, the TWR must be minimized but the priority of maximization of MRR is more than that. After several analysis with the different target values of TWR including the least value, the above said value which is approximately average of all the TWR has been found suitable for the optimization. The constraints were taken as upper and lower and upper value of each input parameter. At two sided confidence level of 95% the calculation was performed.

3.5.1. Result of optimization

Using MINITAB 17.0, the result of the optimization is achieved and enlisted in Table 10. The value of MRR, TWR and SR for the optimal setting of parameters are 26.1358 mm^3/min, 0.08 mm^3/min and 5.8182 µm respectively. The value of composite desirability is found 0.8398 as shown in Fig. 10. It indicates that the degree of optimization has achieved closer to 1 and supports for accepting the result.

Table 10. Result of multi objective optimization using desirability function

Input parameters	Optimized result	MRR	TWR	SR
I (A)	8.6082			
P_{on} (µs)	35.0			
DC	0.5029	26.1358 mm^3/min	0.0800 mm^3/min	5.8182 µm
C_p (g/l)	8.0			
M (µm)	35.0			

3.5.2. Validation of the result

The result of the optimization has been validated by conducting a validation experiment. In this experiment, input parameters were set with the feasible value correspond to the optimal set of solution achieved from the optimization. The input parameters selected for the validation test were current as 9 A, pulse on time as 35 µs, duty cycle as 0.5, powder concentration as 8 g/l and mesh size 35 µm. The other input parameters and experimental environment were kept unaltered as done the main experiment. The responses were measured in the way same as measured previously. The values of MRR, TWR and SR are 25.864 mm^3/min, 0.0836 mm^3/min and 6.21 µm. Therefore, a percentage relative error of the prediction is calculated against the actual result and found the errors for MRR, TWR and SR are 1.03%, 4.50% and 6.73%. A similar type multi objective optimization has been performed to optimize the PMEDM process of H11 steel. It is found that the confirmatory test result of MRR, TWR and SR has been deviated from the optimized result by less than 8% for each responses [33]. However, it is enough to accept the optimized result in the practical application having the same affecting parameters with same level values.

3.6. AFM study of the surface

Atomic force microscopy (AFM) is used to capture the three dimensional surface morphology of the machined surface using interatomic van der Waal force. In this measurement, a very sensitive cantilever beam attached with a silicon tip of 10 nm is moved on the surface by making direct contact [39, 40]. The precise deflection of the beam is measured and sensed by an electronic sensor and the three dimensional image of the surface is generated. From the AFM images, the vertical projections are measured in nanoscale and the surface roughness can be calculated from the data. In the current study, the machine surface were analyzed by the scanning of a small area under AFM probe and the surface roughness has been calculated from the morphological data. A comparative study has been made to analyze the changes in surface roughness with the increase of current. Therefore, three samples from the experimental run viz. sample no 26, 16 and 23 concerning with the current level of 4 A, 8 A and 12 A have been studied under the atomic force microscopy. Fig. 11 (a)-(c) represents the 3D AFM image of the samples. The scanning was done for sample no. 26 and 16 on the area of 80 µm × 80 µm whereas for sample no. 23, it was measured on 25 µm × 25 µm. The surface roughness calculated from the measured data for the sample machined by current levels 4 A, 8 A and 12 A are 4.96 µm, 8.78 µm and 10.94 µm respectively. The deviations of the SR value measured by AFM to that from surface profilometer are 17.30%, 3.64% and 6.21%. The deviation for all the measurements are less than 20%. Nevertheless the result indicates the measurements taken by AFM and surface profilometer is much closer to each other. The wide deviation of the measured value can be explained by inevitable errors during the measurements in both the instruments. Especially in AFM, external vibration and unavoidable gap between the probe and the surface causes significant error in measurements [41]. Also the surface roughness measured by surface profilometer is a measurement made by traversing the probe in a line which must be deviated to some extent from the AFM measurement performed in a small area as it has slightly different characteristics of roughness than a line.

Figure 10. Result of multi objective optimization by desirability function approach

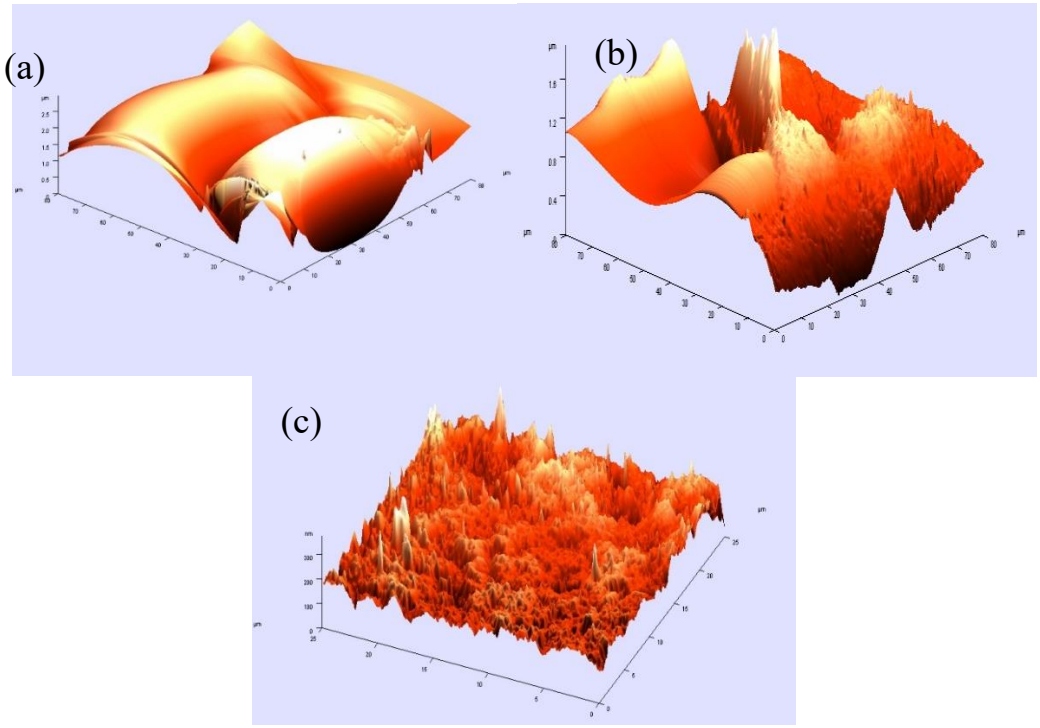

Figure 11. AFM analysis of the machined surfaces at (a) 4 A (b) 8 A and (c) 12 A

3.7. Surface morphology studies

In this section, study of the machined surface morphology has been discussed in qualitative and quantitative approach. Field effect scanning electrode microscope (FESEM: model: Sigma Smart Sem, version 5.09, maker's name: Carl Zeiss Microscopy Ltd.) was used to capture the micrograph of the surface. The overall surface integrity and depositions were analyzed in 500× magnification and the detail crack width measurement was performed in 5000× magnification.

Fig. 12 (a), (c) and (e) represent the small magnification surface micrographs for the samples machined by a current of 4 A, 8 A and 12 A respectively. As per the qualitative investigations are concerned, it is clearly observed the surface consists irregular and complex shaped recast layers, deposition of powder particles in the form of globules and microcracks. The recast layers are formed due to the deposition of the molten material on the surface. After melting, an adhesive force acts between the detached molten material and the hot and newly generated surface. This adhesive force cannot be absolutely overtaken by the flushing force of dielectric flow and as a result the recast layers deposit on the surface itself. During the discharge several phenomenon occurs at the spark gap. Out of them, one important phenomenon is the random movement of powder particles during the electrical discharge. The movement of the particles cause several plastic collision with molten material and deposited on the surface in the form of globules. These globules are extremely hard and deposited randomly on the surface as shown in white color in Fig. 12. In this study, since current is the major influencing parameter, the micrographs of the machine surface were taken for the three levels of the current. From the above said figures, it is observed that the recast layer enhances and more microparticles deposit with the increase of current. As the current increases, high energy discharges are applied by electrode and powder particles. It helps to deposit the material at faster rate than the discharge made by low value of current. Hence the spreading of recast layer increases. On the other hand, at high energy discharge the powders are deflected far from the spark gap with the help of plasma pressure which prevents the formation of globules and reduces the deposition on the surface.

Fig. 12 (b), (d) and (f) represent the magnified view of the surface focusing the microcracks on it. The cracks are generated due to the thermal stress formed when sudden contraction takes place during the cooling period. Also the formation of hard recast layer on the surface creates the thermal stress. Due to which, the cracks are normally found at the periphery of the recast layer. The quantitative analysis was done on each surface by measuring the crack width at two arbitrary points of the crack and shown the average of the measurement on the figures. The average crack width are found 1.151 µm, 1.568 µm and 1.865 µm for 4 A, 8 A, 12 A respectively. As discussed earlier, high thermal energy generates when current increases and the thermal stress developed on the surface increases. This causes severe contraction on the surface. As a result, the crack width increases with the increase of current value. Controlling the current at optimum level and increasing the graphite concentration can reduce the width of the microcracks.

3.8. Analysis of XRD pattern

Fig. 13 represents the X-ray diffraction (XRD) study of different crystallographic planes present in Inconel 625 machined surface. The super alloy consists mainly two phases. Such as γ austenitic phase consists the solid solution of iron and chromium in nickel matrix (Ni-Fe-Cr) and γ'' intermetallic precipitating phase consists Ni_3Nb phase [42]. In the Fig. 13 (a), different XRD patternshave been plotted against 2θ angel ranged from 0^0 to 80^0 for the samples machined by three levels of current. The peaks correspond to the lattice plane of (111), (200) and (220) are identified for all the three samples and it consists both the matrix and intermetallic phases of the alloys [42]. From the Fig. 13(a), it is observed that the peaks are placed at their proper position which determines there is no severe deformation takes place in the crystallographic planes during the machining. But a little right shift is observed in all the peaks which indicates a little deformation occurs in crystal structures.

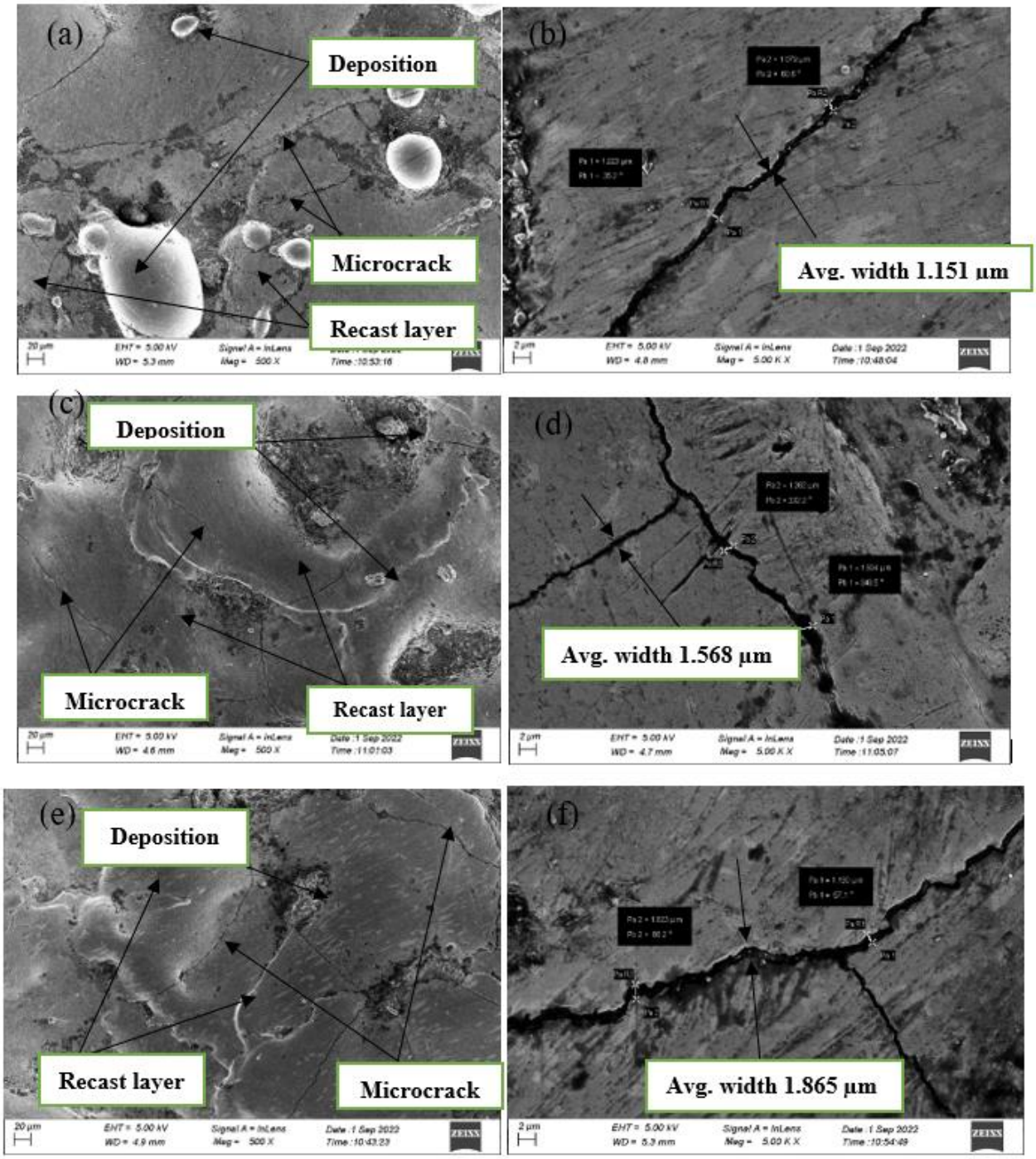

Figure 12. SEM micrography of the machined surface generated at 4 A with a magnification of (a) 500× and (b) 5000×; at 8 A with a magnification of (c) 500× and (d) 5000× and at 12 A magnification of (e) 500× and (f) 5000×.

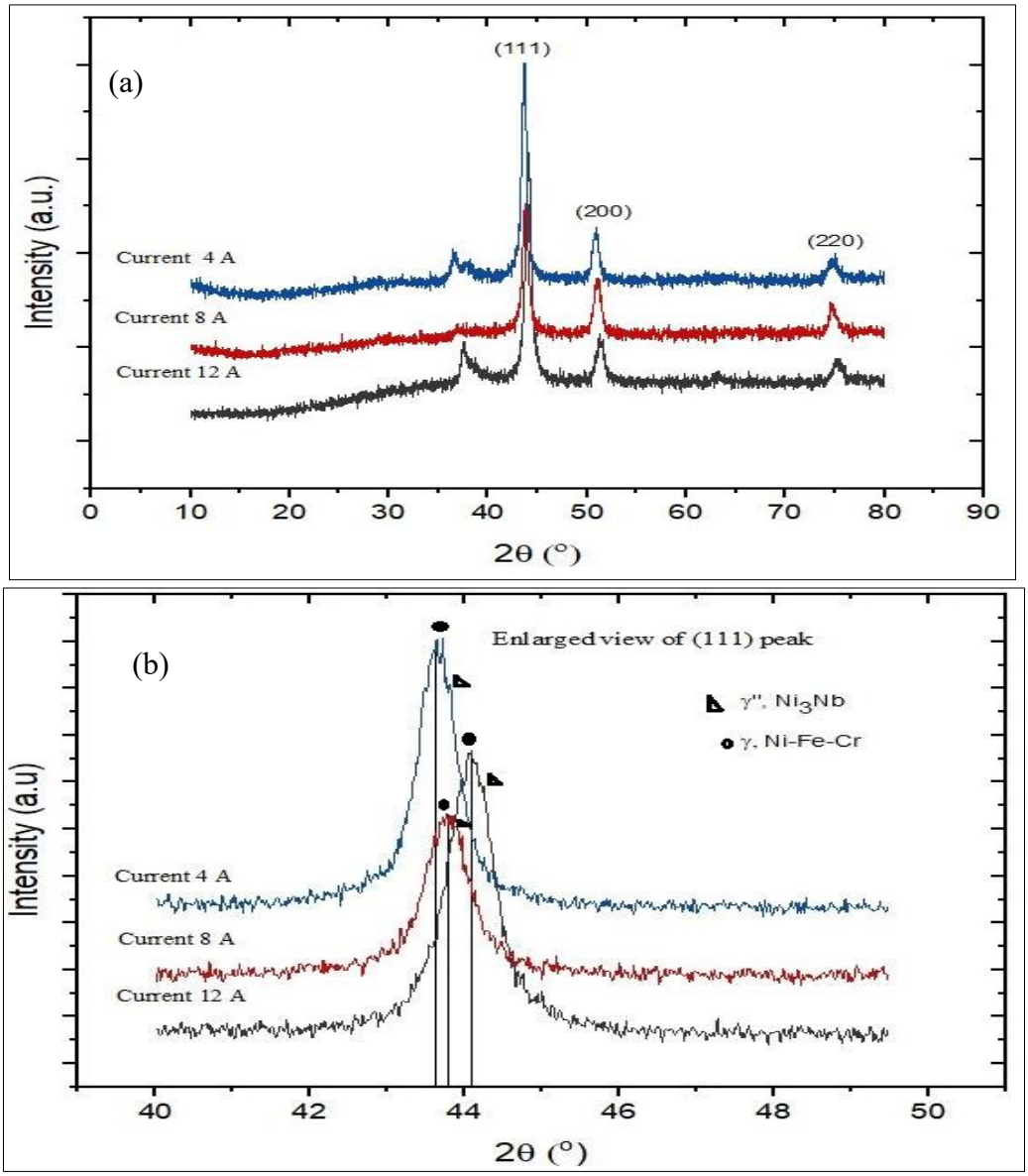

Figure 13. XRD pattern of samples machined under 3 levels of current showing (a) complete view of all the planes (b) enlarged view of (111) plane

However, an enlarged view of the lattice plane (111) has further been plotted and shown in Fig. 12 (b). In the figure, it can be investigated that the peaks have been shifted at right side continuously when the current increases from 4 A to 12 A. The right shift of the peak implies the angle of diffraction for the particular lattice plane has been increased. According to Bragg's law, increase of angle reduces distance of the lattice planes. This can beexplained as the formation of lattice distortion caused by increased internal energy of the crystal structure. During the machining, when current increases the energy of the electrical spark also increases. This increases the temperature of the surface which is responsible for the vibration of the atoms at higher frequency and longer period of time. During this time, atoms having large atomic radius like niobium, molybdenum get dissociated from the crystal structure and small atoms like chromium and iron occupy the void portion [43]. In this way, the lattice distance reduces and a slight transformation from ɤ'' or Ni_3Nb double austenitic phase to ɤ or Ni-Fe-Cr single austenite phase has happened when the increases during the machining. However, the changes of phases is very small which does not affect the ratio of two phases of the alloy.

4. Conclusion

In the present study, the processing of Inconel 625 using graphite mixed electric discharge machining has been investigated by the ANN predictive model and RSM desirability optimization approach. Along with these, the study of surface characteristics and phase analysis after machining have been performed using AFM, FESEM and XRD analysis. The conclusion of the above study can be drawn in following way-

Firstly, the effects of graphite powder have been investigated on the MRR, TWR and SR after machining in EDM. Since the electrical conductivity of graphite is high, addition of its powder in the dielectric fluid increases the induced electrical energy in the discharge column and the material removal enhances. Along with that the uniform discharge and reduction of temperature on the electrode surface reduces the SR and TWR respectively. The study clearly indicates that the addition of powder improves all the responses continuously which in turns conclude that compare to normal EDM, graphite mixed EDM can enhance the productivity and quality during the Inconel 625 processing.

The ANOVA result of this study found that current and powder concentrations are the common significant parameters for all the responses viz. MRR, TWR and SR. Also, the square of the current and the conjugate interaction of current and powder concentration are found significant for them. The analysis further found that an improvement of all the output parameters had happened mostly by increasing the current and the graphite concentration during the machining. The RSM regression model for all the responses are found adequate since the R^2 value for each equation is around 90%. The p values of lack of fit test during ANOVA of three responses came greater than 0.05 which determined the RSM model fits the experimental data satisfactorily.

The 3 layer ANN model provides an outstanding predictive model for the prediction of all the responses. The mean error of prediction by this network for MRR, TWR and SR are 5.95%, 7.30% and 6.40% respectively. R value of the model was found at 0.94509. However, the accuracy of the ANN model is found satisfactory and can be accepted for the prediction in industrial application. The convergence of the model reaches at a very small computational time with 11 epochs only.

Using desirability function approach, the optimal solution of MRR, TWR and SR has been derived at current = 8.6082 A, pulse on time = 35 µs, duty cycle = 0.5029, powder concentration = 8 g/l and mesh size 35 µm. The value of MRR, TWR and SR is 26.1358 mm^3/min, 0.08 mm^3/min and 5.8182 µm. The validation test has been conducted with the nearest possible valuesand found the deviationsas 1.03%, 4.50% and 6.73% for MRR, TWR and SR respectively. The closeness of the optimize result with validation test makes the optimization process adequate to use in the practical field.

In the SEM micrography, it has been observed that the recast layer density increases and the deposition of globules decreases with the increase of current. The width of the micro-crack has also been increased with the increase of current. Analysis of XRD pattern reveals that a little right shift has been observed for each peak of the crystallographic plane. The further analysis confirms that a small transformation from Ni_3Nb to Ni-Cr-Fe austenitic had happened at the higher value of current due to the shifting of niobium from the lattice structure.

Acknowledgement

The authors are grateful to Heritage Institute of Technology for permitting the use of their EDM and the additional setup. Further, the authors would like to acknowledge NIT, Durgapur for providing the SEM and XRD results analyzed on the samples.

Conflict of interest

The authors are declaring that there exist no single conflict of interest among themselves.

References

[1] D. Dudzinski, A. Devillez, A. Moufki, D. Larrouquere, V. Zerrouki, J. Vigneau, “A review of developments towards dry and high speed machining of Inconel 718 alloy”. International journal of machine tools and manufacture,Vol. 44, 2004, 439-456.https://doi.org/10.1016/S0890-6955(03)00159-7

[2] E. Hosseini, V. A. Popovich,“A review of mechanical properties of additively manufactured Inconel 718”. Additive Manufacturing, Vol. 30, 2019, 1-18. https://doi.org/10.1016/j.addma.2019.100877

[3] H. Dong, Y. Liu, Y. Shen, X. Wang, “Optimizing machining parameters of compound machining of Inconel 718” . Procedia CIRP, Vol. 42, 2016, 51-56. https://doi.org/10.1016/j.procir.2016.02.185

[4] M. Gangil, M. K. Pradhan, “Modeling and optimization of electrical discharge machining process using RSM: A review”. Materials Today: Proceedings, Vol. 4, 2017, 1752-1761. https://doi.org/10.1016/j.matpr.2017.02.017

[5] R. V. S. Subrahmanyam, K. Ramji, P. S. Rao, C. V. Rao, “The Analysis of Particle Size Effect on Performance of WC/Cu P/M Compact Sintered Electrode in EDM Process”. Jordan Journal of Mechanical and Industrial Engineering, Vol. 15, 2021, 451-460.

[6]J. E. Qudeiri, A. Saleh, A. Ziout,, A. H. I. Mourad, A, M. H. Abidi, A. Elkaseer, “Advanced electric discharge machining of stainless steels: Assessment of the state of the art, gaps and future prospect”. Materials, Vol. 12, 2019, 907. https://doi.org/10.3390/ma12060907

[7] K. H. Ho, S. T. Newman, “State of the art electrical discharge machining (EDM)”. International journal of machine tools and manufacture, Vol. 43, 2003, 1287-1300. https://doi.org/10.1016/S0890-6955(03)00162-7

[8] Davim JP. Nontraditional machining processes. London: springer-Verlag; 2013.

[9]A. Y. Joshi, A. Y. Joshi,“A systematic review on powder mixed electrical discharge machining”. Heliyon,Vol. 5, 2019, 1-12. https://doi.org/10.1016/j.heliyon.2019.e02963

[10] S. Majumdar, N. K. Bhoi, H. Singh, “Graphene nano-powder mixed electric discharge machining of Inconel 625 alloy: optimization of process parameters for material removal rate”. International Journal onInteractive Design Manufacturing, 2022. https://doi.org/10.1007/s12008-022-00996-w

[11] G. Talla, S. Gangopadhyay, C. K. Biswas, “Effect of powder-suspended dielectric on the EDM characteristics of Inconel 625”. Journal of Materials Engineering and Performance, Vol. 25, 2016, 704-717.

[12] P. Pecas,E. Henriques,“Electrical discharge machining using simple and powder-mixed dielectric: the effect of the electrode area in the surface roughness and topography”. Journal of materials processing technology, Vol. 200, 2008, 250-258. doi:10.1016jmatprotec.2007.09.051

[13] M. Kolli, A. Kumar,“Effect of dielectric fluid with surfactant and graphite powder on Electrical Discharge Machining of titanium alloy using Taguchi method”. Engineering Science and Technology, an International Journal, Vol. 18, 2015, 524-535. http://dx.doi.org/10.1016/j.jestch.2015.03.009

[14] H. Marashi, A. A. Sarhan, M. Hamdi, “Employing Ti nano-powder dielectric to enhance surface characteristics in electrical discharge machining of AISI D2 steel”. Applied surface science, Vol. 357, 2015, 892-907. http://dx.doi.org/10.1016/j.apsusc.2015.09.105

[15] P. J. Liew, J. Yan, T. Kuriyagawa,“Carbon nanofiber assisted micro electro discharge machining of reaction-bonded silicon carbide”. Journal of Materials Processing Technology, Vol. 213, 2013, 1076-1087. http://dx.doi.org/10.1016/j.jmatprotec.2013.02.004

[16] G. Talla, S. Gangopadhayay, C. K. Biswas,“Multi response optimization of powder mixed electric discharge machining Aluminium/ Alumina metal matrix composite using Grey Relation Analysis”. Procedia Materials Science, Vol. 5, 2014, 1633-1639. doi: 10.1016/j.mspro.2014.07.351.

[17] J. Anitha, R. Dasa, M. K. Pradhan, “Multi-objective optimization of electrical discharge machining processes using artificial neural network”. Jordan Journal of Mechanical and Industrial Engineering, Vol. 10, No. 1, 2016, 11-18.

[18] A. K. Rouniyar, P. Shandilya,“Fabrication and experimental investigation of magnetic field assisted powder mixed electrical discharge machining on machining of aluminum 6061 alloy”. Proceedings of the Institution of Mechanical Engineers, Part B: Journal of Engineering Manufacture, Vol. 233, 2019, 2283-2291. DOI: 10.1177/0954405419838954.

[19] S. K. Sahu,S. Datta,“Experimental studies on graphite powder-mixed electro-discharge machining of Inconel 718 super alloys: comparison with conventional electro-discharge machining”.

Proceedings of the Institution of Mechanical Engineers, Part E: Journal of Process Mechanical Engineering, Vol. 233, 2019, 384-402. DOI: 10.1177/0954405419838954.

[20] Y. S. Kim, C. N. Chu,"The effects of graphite powder on tool wear in micro electrical discharge machining". Procedia CIRP, Vol. 68, 2018,553-558. doi: 10.1016/j.procir.2017.12.121

[21] S. Jarin, T. Saleh, M. Rana, A. G. Muthalif, M. Y. Ali,"An experimental investigation on the effect of nanopowder for micro-wire electro discharge machining of gold coated silicon". Procedia engineering, Vol. 184, 2017, 171-177. doi: 10.1016/j.proeng. 2017.04.082

[22] Y. S. Wong, L. C. Lim, I. Rahuman, W. M. Tee,"Near-mirror-finish phenomenon in EDM using powder-mixed dielectric". Journal of Materials Processing Technology, Vol. 79, 1998, 30-40.https://doi.org/10.1016/S0924-0136(97)00450-0

[23] Z. J. Xie, Y. J. Mai, W. Q. Lian, S. L. He, X. H. Jie,"Titanium carbide coating with enhanced tribological properties obtained by EDC using partially sintered titanium electrodes and graphite powder mixed dielectric". Surface and Coatings Technology, Vol. 25, 2016, 50-57.http://dx.doi.org/10.1016/j.surfcoat.2016.04.080

[24] S. P. Dwivedi, R. Sahu, "Effects of SiC Particles Parameters on the Corrosion Protection of Aluminum-based Metal Matrix Composites using Response Surface Methodology". Jordan Journal of Mechanical and Industrial Engineering, Vol. 12, No. 4, 2018, 313-321.

[25] M. Rahimi, H. Fazlollahtabar, "Optimization of a Closed Loop Green Supply Chain using Particle Swarm and Genetic Algorithms". Jordan Journal of Mechanical and Industrial Engineering, Vol. 12, No. 2, 2018, 77-91.

[26] R. Das, M. K. Pradhan, C. Das, "Prediction of surface roughness in Electrical Discharge Machining of SKD 11 TOOL steel using Recurrent Elman Networks". Jordan Journal of Mechanical and Industrial Engineering, Vol. 7, 2013, 67-71.

[27] M. T.Hayajneh, M. Abdellahia, "Prediction Performance of End-Milling Process by Gene Expression Programming". Jordan Journal of Mechanical and Industrial Engineering, Vol. 13, 2019, 83-89.

[28] A. H. Q. Ayun, J. Triyono, E. Pujiyanto, E, "Optimization of injection molding simulation of bioabsorbable bone screw using Taguchi method and particle swarm optimization". Jordan Journal of Mechanical and Industrial Engineering, Vol. 16, 2022, 319-325.

[29] D. Sharma, A. Bhowmick, A. Goyal,"Enhancing EDM performance characteristics of Inconel 625 superalloy using response surface methodology and ANFIS integrated approach". CIRP Journal of Manufacturing Science and Technology, Vol. 37, 2022, 155-173.

[30] S. Bhowmick, R. Mondal, S. Sarkar, N. Biswas, J. De, G. Majumdar,"Parametric optimization and prediction of MRR and surface roughness of titanium mixed EDM for Inconel 718 using RSM and fuzzy logic". CIRP Journal of Manufacturing Science and Technology, Vol. 40, 2023, 10-28.

[31] K. Kadirgama, M. M. Noor, M. M. Rahman, "Optimization of surface roughness in end milling on mould aluminium alloys (AA6061-T6) using response surface method and radian basis function network". Jourdan Journal of Mechanical and Industrial Engineering, Vol. 2, 2008, 209-214.

[32] F. Sk, D. V. Kumar, "Optimization of Performance and Exhaust Emissions of a PFI SI Engine Operated with Iso-stoichiometric GEM Blends Using Response Surface Methodology". Jordan Journal of Mechanical and Industrial Engineering, Vol. 15, 2021, 199-207.

[33] T. Le,"Surrogate neural network model for prediction of load-bearing capacity of CFSS members considering loading eccentricity". Applied Sciences, Vol. 10,2020, 1-22. doi:10.3390/app10103452

[34] F. B. Ismail, A. Al-Bazi, R. H. Al-Hadeethi, M. Victor, "A Machine Learning Approach for Fire-Fighting Detection in the Power Industry". Jordan Journal of Mechanical and Industrial Engineering, Vol. 15, 2021, 475-482.

[35] P. Sreeraj, T. Kannan,"Modelling and prediction of stainless steel clad bead geometry deposited by GMAW using regression and artificial neural network models". Advances in Mechanical Engineering, Vol.4, 2012, 1-12.doi:10.1155/2012/237379

[36]S. Tripathy, D. K. Tripathy, "Multi-attribute optimization of machining process parameters in powder mixed electro-discharge machining using TOPSIS and grey relational analysis". Engineering Science and Technology, an International Journal, Vol. 19, 2016, 62-70. DOI: http://dx.doi.org/ 10.1016/j.jestch.2015.07.010

[37] S. G. Ghalme, "Improving Mechanical Properties of Rice Husk and Straw Fiber Reinforced Polymer Composite through Reinforcement Optimization". Jordan Journal of Mechanical and Industrial Engineering, Vol. 15, 2021, 411-417.

[38] N. Faisal, K. Kumar, "Optimization of machine process parameters in EDM for EN 31 using evolutionary optimization techniques". Technologies, Vol. 6, No. 2, 2018, 1-16. doi:10.3390/technologies6020054

[39] S. Prabhu, B. K. Vinayagam, "AFM surface investigation of Inconel 825 with multi wall carbon nano tube in electrical discharge machining process using Taguchi analysis". Archives of civil and mechanical engineering 11, 2011, 149-170. https://doi.org/10.1016/S1644-9665(12)60180-0

[40] Y. H. Guu, M. T. Hou, "Effect of machining parameters on surface textures in EDM of Fe-Mn-Al alloy". Materials Science and Engineering: A, Vol. 466, 2007, 61-67. doi:10.1016/ j.msea.2007.02.035

[41] C. Y. Poon, B. Bhushan, "Comparison of surface roughness measurements by stylus profiler, AFM and non-contact optical profiler". Wear, Vol. 190, 1995, 76-88. https://doi.org/ 10.1016/0043-1648(95)06697-7

[42] S. Li, Q. Wei, Y. Shi, Z. Zhu, D. Zhang, "Microstructure characteristics of Inconel 625 superalloy manufactured by selective laser melting". Journal of Materials Science & Technology, Vol. 31,2015, 946-952. http://dx.doi.org/10.1016 /j.jmst.2014.09.020

[43] X. Liu, K. Wang, P. Hu, X. He, B. Yan, X. Zhao, "Formability, microstructure and properties of inconel 718 superalloy fabricated by selective laser melting additive manufacture technology". Materials, Vol. 14, 2021, 1-17. https://doi.org/10.3390 /ma14040991